Biomaterials 160 (2018) 107–123

Contents lists available at ScienceDirect

Biomaterials

journal homepage: www.elsevier.com/locate/biomaterials

Azithromycin-loaded respirable microparticles for targeted pulmonary delivery for the treatment of pneumonia

Qiyue Wang [a], Gujie Mi [b], Daniel Hickey [b], Yanan Li [a], Jiasheng Tu [a, *], Thomas J. Webster [b, **], Yan Shen [a, ***]

[a] Center for Research Development and Evaluation of Pharmaceutical Excipients and Generic Drugs, Department of Pharmaceutics, China Pharmaceutical University, 24 Tong Jia Xiang, Nanjing 210009, China
[b] Department of Chemical Engineering, Northeastern University, 360 Huntington Avenue, Boston, MA 02115, United States

ARTICLE INFO

Article history:
Received 16 November 2017
Received in revised form
4 January 2018
Accepted 14 January 2018

Keywords:
Fumaroylated diketopiperazine
Azithromycin
Pulmonary delivery
Microparticles
Pneumonia

ABSTRACT

Pneumonia is a major contributor to infection-based hospitalizations and deaths in the United States. Antibiotics such as azithromycin (AZM), although effective at managing pneumonia, often suffer from off-target diffusion and poor bioavailability when administered orally or via intravenous injection. The formation of biofilms at the disease sites makes the treatment more complicated by protecting bacteria from antimicrobial agents and thus necessitating a much higher dosage of antibiotics to eradicate the biofilms. As such, targeted pulmonary delivery of antibiotics has emerged as a promising alternative by providing direct access to the lung while also allowing higher local therapeutic concentrations but minimal systemic exposure. In this study, AZM was encapsulated in N-fumaroylated diketopiperazine (FDKP) microparticles for efficient pulmonary delivery. Both *in vitro* and *in vivo* results demonstrated that AZM@FDKP-MPs administered via intratracheal insufflation achieved at least a 3.4 times higher local concentration and prolonged retention times compared to intravenous injection and oral administration, suggesting their potential to better manage bacterial pneumonia.

1. Introduction

Pneumonia is a major contributor to infection-based hospitalizations and deaths among all age groups in the United States, and is responsible for 4 million deaths worldwide every year [1,2]. Even with the introduction of pneumococcal conjugate vaccines, pneumonia has continued to be the eighth most expensive condition treated in hospitals nationwide with an estimated economic burden exceeding $\$1.62 \times 10^{10}$ in 2013 [3,4]. Pneumonia is most commonly caused by viruses or bacteria such as *S. pneumoniae*, with bacteria being the most common cause of community-acquired pneumonia (CAP) [5,6]. In the case of bacterial pneumonia, the macrolide drug azithromycin (AZM), a semi-synthetic 9-N-methylation derivative of erythromycin, is typically recommended in the United States as a first-line outpatient treatment, or as part of a combination therapy in patients who require hospitalization [7–9]. AZM is a broad-spectrum antibiotic useful for the treatment of a number of gram-positive, gram-negative, and atypical bacterial infections that lead to pneumonia, such as those caused by *S. pneumoniae*, *haemophilus influenza*, and *clamydophila pneumoniae* [10,11]. The most common routes of administration of AZM to treat pneumonia are orally, by intravenous injection, or by intravenous infusion [12]. Although generally effective and sufficient for managing bacterial pneumonia, these systemic delivery methods will inevitably lead to off-target diffusion, poor bioavailability and, consequently, higher doses to attain the necessary concentrations in the lung, especially in the epithelial lining fluid. Considering that AZM was the most prescribed antibiotic for outpatients in the US in 2010 [13], the threat of developing bacterial resistance is a concern. Moreover, bacteria such as *S. pneumoniae* tend to form biofilms that protect them from antimicrobial agents and host immune responses. These are a result of changes in metabolic processes or poor antimicrobial diffusion and could increase antibiotic resistance hundreds of times compared to planktonic bacteria [14–17]. The targeted pulmonary delivery of AZM in the form of dry powders provides direct access to the lungs,

* Corresponding author.
** Corresponding author.
*** Corresponding author.
E-mail addresses: jiashengtu@aliyun.com (J. Tu), th.webster@neu.edu (T.J. Webster), shenyan19820801@126.com (Y. Shen).

https://doi.org/10.1016/j.biomaterials.2018.01.022
0142-9612/

supplying increased local therapeutic concentrations with minimal systemic exposure. Collectively, these characteristics decrease the chance that bacteria will develop antibiotic resistance [18] [19]. As such, targeted pulmonary delivery has become an attractive method of managing lower respiratory tract infections. In addition, the advances in dry powder inhalers make this route of drug administration more efficient and more convenient for patients [20].

The large surface area, thin alveolar epithelium and lack of first-pass metabolism are all beneficial for efficient drug absorption in the lung [21]. As a major port of entry, however, the lung has evolved to protect the airways from exposure to unwanted foreign materials via phagocytic and mucociliary clearance. While this feature is effective in protecting the body from foreign invasion, it represents a significant barrier for pulmonary drug delivery [20]. Consequently, engineering particles that can achieve effective aerosolization, maximize lung deposition, and minimize macrophage uptake is of the utmost importance for effective pulmonary delivery [22]. Towards this end, optimization of the aerosolization performance of dry powders is dependent on several factors [23]. First, aerodynamic particle size and size distribution can significantly impact the delivery of the particles throughout the lung. For example, previous research has shown that optimal deep lung deposition can be achieved with particles ranging from 1 to 5 μm [24]. Second, surface morphology and hygroscopicity have been shown to influence particle flow and atomization behavior [25–31]. Previous studies have demonstrated that corrugated particles with rougher surfaces may contribute to van der Waals force changes between particles [32]. The hygroscopicity of drugs and excipients has also been shown to play a role in aerosol generation and lung deposition by altering moisture absorption capacities, which may lead to particle dissolution or aggregation [33]. Finally, excipients are frequently incorporated as carriers or extenders to improve aerosolization properties. For pulmonary drug delivery, excipients should be well-tolerated and have short retention times in the lung. Common excipients used for pulmonary drug delivery can be divided into three categories: (1) sugars, such as lactose, mannitol, and glucose, which were once the most widely used excipients with favorable safety profiles. Unfortunately, sugar-based excipients usually result in large particle sizes and can adversely affect particle lung deposition. This could lead to lower drug accumulation in the lung and eventually compromise effectiveness. (2) Lipids, such as 1,2-dipalmitoyl-*sn*-glycero-3-phosphocholine (DPPC), 1,2-distearoyl-*sn*-glycero-3-phosphocholine (DSPC), and cholesterol, are endogenous substances in the lung and can be further modified to improve aerosolization properties. Dosage forms like liposome and solid lipid microparticles (SLM) have been shown to improve drug retention time and reduce toxicities. However, the relatively high price of lipids have hindered their wide application as pulmonary delivery excipients. (3) Biodegradable polymers such as PLGA have also been widely investigated as pulmonary delivery vehicles due to their good lung deposition ability. However, PLGA could easily degrade into acidic products such as lactic acid and glycolic acid in the lung and the accumulation of acidic degradation products may cause long-term respiratory irritations and could eventually lead to adverse immune responses in the lungs resulting in cough, edema and neutrophil infiltration.

Towards this end, fumaryl diketopiperazine (FDKP) is an FDA-approved, inert excipient that has been used as the primary component in Afrezza® to assist in the delivery of recombinant human insulin via inhalation [34,35]. FDKP possesses two carboxyl groups and undergoes acid-induced intermolecular self-assembly in acidic environments (pH < 5) to form microparticles with a negatively charged surface [36]. Protein or small molecule therapeutics with positive charges at acidic pH can therefore be adsorbed onto the surface of FDKP microparticles via electrostatic interactions. Furthermore, dry powders of drug-loaded FDKP microparticles can be obtained upon spray drying. Once deposited into the lung, FDKP microparticles can dissolve at neutral pH and release drugs rapidly. The FDKP is then distributed to other tissues and excreted from the kidney in its original form [36].

In this study, FDKP was successfully synthesized and characterized as a safe excipient to deliver AZM into the lung. FDKP microparticles (FDKP-MPs), AZM microparticles (AZM-MPs) and AZM loaded FDKP microparticles (AZM@FDKP-MPs) were formulated and compared for their physicochemical properties as well as their aerodynamic behaviors to optimize the effectiveness of pulmonary delivery. AZM@FDKP-MPs exhibited fantastic aerosolization performance, improved moisture resistance and, most importantly, exceptional deep lung deposition. *In vitro* antibacterial experiments were carried out to confirm that the addition of FDKP had no impact on the minimum inhibitory concentration (MIC) of AZM for *S. pneumonia.* Finally, pharmacokinetic and pharmacodynamic studies were conducted in a pneumonia mouse model to explore whether the use of inhalable AZM@FDKP-MPs reduced the frequency of administration and/or was more effective in reversing disease progression compared to oral administration or intravenous injection. Our findings *in vivo* clearly suggest that AZM@FDKP-MPs administered via intratracheal insufflation achieved the highest local concentration and prolonged retention time and could, thus, be a successful and novel pneumonia treatment.

2. Materials and methods

2.1. Materials and animals

N_6-trifluoroacetyl-L-lysine was purchased from Adamas-beta® (Shanghai, China); 1-ethyl-3-(3-dimethylaminopropyl)carbodiimide hydrochloride (EDC) and N-Hydroxysuccinimide (NHS) were obtained from Aladdin® (Shanghai, China); Fumaric acid monoethyl ester was acquired from Dingchem™ (Shanghai, China); and azithromycin (AZI) was supplied by Jiangchuan pharmaceutical Co., Ltd (Chengdu, China). All other reagents, if not specified, were purchased from Sinopharm Chemical Reagent Co., Ltd and were of analytical grade.

Female normal mice and BALB/c mice ($w = 18–22$ g) were purchased from the Experimental Animal Center of Nanjing Qinglongshan. All animal experiments were conducted in accordance with the Guide for Laboratory Animal Facilities and Care and were approved by the Animal Ethics Committee of China Pharmaceutical University.

2.2. Synthesis of fumaryl diketopiperazine (FDKP)

The FDKP was synthesized using a three-step reaction. Briefly, 10 g of N_6-trifluoroacetyl-L-lysine and 1.76 g of phosphorus pentoxide were dissolved in 50 mL of N-methyl-2-pyrrolidinone (NMP) in a three-neck flask and were allowed to react at 165 °C for 1.5 h under nitrogen protection and constant stirring. The reaction mixture was cooled to room temperature and poured into 1000 mL of deionized water to allow for precipitation. The precipitates were washed twice with deionized water and were vacuum dried for 24 h to obtain trifluoroacetyl-diketopiperazine (TFA-DKP) [37]. TFA-DKP was then hydrolyzed using a 5% sodium hydroxide solution to remove the trifluoroacetyl group and then added dropwise into an active ester solution formed by EDC, NHS and fumaric acid monoethyl ester. The mixture was allowed to react for 24 h with a pH adjusted to around 7–8 and was poured into deionized water for precipitation. The precipitates were collected and were further

hydrolyzed using a sodium hydroxide water-methanol (1:1) solution for another 6 h to allow for complete hydrolysis until the solution turned clear. The pH was then adjusted to 2–3 using hydrochloric acid (0.1 M) to allow for the precipitation of FDKP, and the precipitates were then collected by filtration. To further purify the product, three more cycles of precipitation were carried out and the final product was vacuum dried at 60 °C to obtain FDKP powders.

2.3. Preparation of AZM microparticle powders (AZM-MPs), FDKP microparticle powders (FDKP-MPs) and AZM-loaded FDKP microparticle powders (AZM@FDKP-MPs)

An appropriate amount of AZM was dissolved in an acetic acid aqueous solution (1%, *v/v*) and the pH was adjusted to 6.4 due to the stability limitation of AZM using an ammonia solution (1%, *v/v*). Azithromycin microparticle powders (AZM-MPs) were then obtained via spray-drying using the conditions described below.

To prepare FDKP microparticle powders (FDKP-MPs), 150 mg of FDKP was dissolved in 10 mL of an ammonia aqueous solution (1%, *v/v*) and 5 mL of an acetic acid aqueous solution (10%, *v/v*) was added dropwise with a constant flow pump at a speed of 2 mL min^{-1}. The FDKP was precipitated and the suspension was then adjusted to pH 4.5 using an ammonia aqueous solution (1%, *v/v*). The suspension was then homogenized for 8 min at 140 psi to reduce the particle size with a high pressure homogenizer (AH 2010, ATS Engineering Inc., Canada). FDKP-MPs were obtained upon spray-drying.

Azithromycin-loaded FDKP microparticle powder (AZM@FDKP-MPs) was prepared at pH 4.5 and pH 6.4. To prepare AZM@FDKP-MPs at pH 4.5, an appropriate amount (50, 100, and 150 mg) of AZM was dissolved in 2 mL of an acetic acid aqueous solution (pH was adjusted to 4.5 with a 1% (*v/v*) ammonia solution) and was added dropwise into the FDKP suspension (prepared according to the procedures above) under magnetic stirring. The suspension was then spray-dried to obtain AZM@FDKP-MP (pH 4.5). Similarly, AZM@FDKP-MPs at pH 6.4 were prepared by dissolving 100 mg of azithromycin and 150 mg of a FDKP aqueous solution and the pH was adjusted to 6.4 with either acetic acid or ammonia (1%, *v/v*). The mixed solution was finally spray-dried to obtain AZM@FDKP-MP (pH 6.4).

All samples were spray-dried using the following conditions: inlet temperature of 140 °C, aspiration pump rate at 100% (35 m^3 h^{-1}), air atomization flow rate at 600 L h^{-1}, and liquid feed rate at 1.5 mL min^{-1} (5%). Drug loading was calculated according to Equation (1).

$$\text{Drug loading}(\%) = \frac{\text{Drug content in microparticles}}{\text{Quantity of microparticles}} \times 100\% \quad (1)$$

2.4. Particle size and density

The mean particle sizes of spray drying microparticles were measured using a laser diffraction particle size analyzer (BT2001, Jilin better instrument, China). All measurements were done in triplicate (n = 3) at 25 °C and 50% relative humidity.

Carr's index and angle of repose (α) were both used to characterize the flowability of dry powders. AZM-MPs, FDKP-MPs and AZM@FDKP-MPs (pH 4.5 and pH 6.4) powders were filled into a 5-mL cylinder and the volume of the powders was recorded as the bulk volume. The cylinder containing the sample was then tapped mechanically until a further volume change was observed and the final volume of the powder was recorded as the tapped volume. The bulk density (BD), tapped density (TD) and Carr's index were calculated using Equations (2)–(4). The angle of repose was determined by passing a fixed amount of powders through a funnel that was set at a predetermined height and the angles (α) were calculated according to Equation (5):

$$\text{BD} = \frac{\text{Weight of powders}}{\text{Bulk volume}} \quad (2)$$

$$\text{TD} = \frac{\text{Weight of powders}}{\text{Tap volume}} \quad (3)$$

$$\text{Carr's index} = \frac{\text{TD} - \text{BD}}{\text{TD}} \times 100\% \quad (4)$$

$$\tan(\alpha) = \frac{\text{height}}{\text{radius of cone}} \quad (5)$$

In which the height and the radius were the height and the radius accumulated powder cone.

The theoretical aerodynamic diameters of microparticles (D_{aer}) were calculated according to Equation (6):

$$D_{aer} = \sqrt{\frac{TD}{\rho_1}} \times D \quad (6)$$

In which $\rho_1 = 1$ g cm^{-3}; D was the geometric diameter detected by a laser diffraction particle size analyzer.

2.5. Scanning electron microscopy (SEM)

The shape and size of AZM-MPs, FDKP-MPs and AZM@FDKP-MPs (pH 4.5 and pH 6.4) were visualized by scanning electron microscopy (Hitachi SU8010, Hitachi Limited, Japan). The particles were sprinkled onto a double-sided adhesive tape stuck on a silicon stub. The powders were sputter-coated with gold using a Hitachi ion sputter coater (E1010, Hitachi Limited, Japan) and were observed under scanning electron microscopy operating at 15 kV.

2.6. X-ray powder diffraction (XRPD)

XRPD patterns of AZM-MPs, FDKP-MPs and AZM@FDKP-MPs (pH 4.5 and pH 6.4) were investigated at ambient temperature with an X-ray powder diffractometer (D8 Advance, Bruker®, Germany). The powders were loaded onto a horizontal square recess of a sample holder and a razor blade was used to smooth the powder sample evenly into the square. Excess powders were removed from the sides of the sample holder. The surface of the powder should be smooth and level with the sides of the holder by flattening gently with the razor blade and were measured with a slit–detector. The scan was performed at 2.00° min^{-1} over a 2θ range of 3.0–40.0°.

2.7. Differential scanning calorimetry (DSC)

Thermal phase transitions of the particles were analyzed using DSC (DSC 204 HP NETZSCH®, Germany). Briefly, a fixed amount of AZM-MPs, FDKP-MPs and AZM@FDKP-MPs (pH 4.5 and pH 6.4) powders were transferred into an aluminum sample pan which were then hermetically sealed. The powder samples were heated from 40 to 400 °C at a rate of 10 °C·min^{-1}. The ultra-high pure nitrogen was used as the purging gas and the purge rate was set at 50 mL min^{-1}.

2.8. Moisture absorption behavior

Moisture absorption behavior was characterized using a constant room temperature and humidity chamber (SHH-100GD, YSEI, Chong Qing, China). Each formulation was incubated for 24 h at a relative humidity (RH) ranging from 20% to 90% for 24 h. The weight of AZM-MPs, FDKP-MPs and AZM@FDKP-MPs (pH 4.5 and 6.4) powders was determined before and after the moisture absorption experiment.

2.9. Evaluation of aerosol dispersion performance in vitro by the Next Generation Impactor (NGI)

The powder dispersion performance of dry powders was determined using a Next Generation Impactor (NGI, Copley Scientific Limited, Nottingham, UK) equipped with a stainless-steel induction port, USP throat (Copley Scientific Limited, Nottingham, UK) and specialized stainless steel NGI insert impactor stages (Copley Scientific Limited, Nottingham, UK) [30] [38]. The NGI was also coupled with a Copley HCP5 vacuum pump (Copley Scientific Limited, Nottingham, UK) as well as a Copley TPK 2000 critical flow controller (Copley Scientific Limited, Nottingham, UK). The airflow rate was calibrated with a Copley DFM 2000 flow meter (Copley Scientific Limited, Nottingham, UK) before each experiment [38]. 10 mg of AZM-MPs and AZM@FDKP-MPs (pH 4.5 and pH 6.4, respectively) powders were loaded into hydroxypropyl methylcellulose (HPMC) capsules and were subsequently released into the NGI using a dry powder inhalation device (KRT-D01, Charamedical, Tai An, China) with a flow rate of 60 L min^{-1} (to simulate the airflow rate in adults) and a conducting time of 4 s. The effective aerodynamic cutoff diameter ($D_{aer\ 50}$) for each impactor stage at this flow condition was calibrated per the manufacturer's instructions: Stage 1, 8.06 μm; Stage 2, 4.46 μm; Stage 3, 2.82 μm; Stage 4, 1.66 μm; Stage 5, 0.94 μm; Stage 6, 0.55 μm and Stage 7, 0.34 μm. Each stage was covered with 1% (*w/v*) of a Tween 80 solution to trap the particles once they hit the surface of the stages. The particles deposited on the stages were recovered and dissolved in the mobile phase (0.05 M K_2HPO_4–acetonitrile (45:55, *v/v*, pH = 8.2)) and were analyzed for AZM concentration using reverse phase HPLC (Ultimate 3000, Thermo Scientific, US) with a C_{18} column (Agilent Zorbax Extend-C_{18}, 4.6 × 250 mm, 5 μm). The column was maintained at 30 °C and the flow rate of the mobile phase (0.05 M K_2HPO_4–acetonitrile (45:55, *v/v*, pH = 8.2)) was set at 1 mL min^{-1}. AZM was detected by monitoring the absorbance at 210 nm with a UV-detector (VWD-3100, Thermo Scientific, US) and concentrations of AZM on each stage were calculated using a standard curve (A = 21.924c+0.0715, r = 0.9997, linearity range 50 μg mL^{-1} to 300 μg mL^{-1}). The emitted fraction (EF), fine particle fraction (FPF) and respirable fraction (RF) were then calculated by the following Equations (7)–(9):

$$EF(\%) = \frac{ED}{TD} \times 100\% \quad (7)$$

$$FPF(\%) = \frac{FPD}{ED} \times 100\% \quad (8)$$

$$RF(\%) = \frac{FPD}{DD} \times 100\% \quad (9)$$

Where emitted dose (ED) refers to the dose deposited on the device, throat, pre-separator and all impactor stages, total dose (TD) is the amount of powder loaded into the capsules, fine particle dose (FPD) refers to the dose deposited on impactor stage 2–7, and deposited dose (DD) represents the dose deposited on impactor stage 1–7.

Finally, the mass median aerodynamic diameter (MMAD) and the geometric standard deviation (GSD) of the AZM-MPs and AZM@FDKP-MPs (pH 4.5 and pH 6.4) were calculated with online software (MMAD Calculator, 2015) using the NGI data.

2.10. In vitro antibacterial activity of AZM@FDKP-MPs on streptococcus pneumonia

Antibacterial activity of free AZM was compared with those of FDKP and AZM@FDKP-MPs (pH 4.5 and pH 6.4) by determining the minimal inhibitory concentration (MIC) of each formulation. A single isolated *streptococcus pneumonia* (ATCC 49619) colony was removed from its starter plate and inoculated into 5 mL of THY culturing medium (3% Todd-Hewitt + 0.2% Yeast Extract). Inoculated colonies were cultured to late exponential phase in a shaking incubator at 37 °C, 5% CO_2 and then diluted in the media to achieve an absorbance of 0.081 at a wavelength of 630 nm (1.5×10^8 CFU mL^{-1}).

Spectrophotometrically measured bacterial densities were verified by performing colony forming unit assays for the bacterial species used. Bacterial solutions were seeded in a 96-well plate at a density of 1.5×10^5 CFU ml^{-1} and were then co-cultured with AZM or AZM@FDKP-MPs (pH 4.5 and pH 6.4) to obtain a final concentration of AZM ranging from 0.0078 to 4 μg mL^{-1}. FDKP-MPs at a concentration of 6 μg mL^{-1} without AZM incorporation were also included as the control to assess the bactericidal abilities of FDKP. The mixtures were allowed to incubate under constant shaking (100 rpm) at 37 °C for 24 h before measuring the optical density at 630 nm using an ELx800® microplate reader (BioTek Instruments, Inc., Winooski, US). The MIC of each formulation was defined as the lowest concentration that inhibited visible growth of the bacteria after 24 h, and an optical density less than 0.05 was considered as zero bacterial growth in this study.

2.11. Pharmacokinetic study of AZM@FDKP-MPs (pH 4.5) in mice

A total of 126 normal mice were used to evaluate the pharmacokinetics of the AZM@FDKP-MPs. All mice were randomized equally into three groups (n = 42) and were allowed to acclimate for seven days prior to each experiment. Group A was administered with AZI@FDKP-MPs via intratracheal insufflation, group B and group C were dosed through tail vain injection and oral administration, respectively, using a AZM@FDKP-MPs PBS solution (pH 7.4). Dosing was performed at predetermined time intervals and was done on 6 mice at each time interval. To administer AZM@FDKP-MPs by intratracheal insufflation, each mouse was anesthetized with an intraperitoneal injection of 0.25 mL chloral hydrate solution (5%) and was fixed on an oblique plane at an angle of 60°. An endoscope was used to visualize the tracheal opening to assist the insertion of a cannula tube (18 G, 3 cm) and dry powders of AZM@FDKP-MPs (75 mg kg^{-1}) were insufflated with the help of a syringe to ensure the delivery of all powders into the lung. For group B, AZM@FDKP-MPs (75 mg kg^{-1}) was dissolved by PBS (pH 7.4) and was injected via the tail vein. For group C, AZM@FDKP-MPs (75 mg kg^{-1}) was dissolved in PBS (pH 7.4) and was intragastrically administered directly into the stomach.

All mice were sacrificed 0.5, 1, 2, 4, 8, 12 and 24 h after administration and lung tissues were immediately harvested, weighed and homogenized with 1 mL of a sodium hydroxide solution (0.2 M) at 8000 rpm for 1 min using the tissue homogenizer (XHF-D, Scientz, Ning Bo, China). 2 mL of diethyl ether was added into the tissue homogenate and was vortexed for 1 min to extract the AZM. The mixtures were then centrifuged at 8000 rpm for 5 min at 4 °C to allow for separation. The ether phase was transferred into a new

centrifuge tube and was evaporated under N_2 at room temperature. The residues were finally dissolved in a mobile phase (0.01 M KH_2PO_4–acetonitrile (35:65, *v/v*, final pH 9.0)) and the amount of AZM was determined using a pre-validated HPLC method as described before (column temperature at 35 °C; flow rate at 1.0 mL min^{-1} and wavelength at 210 nm).

AZM content was expressed in %ID and was calculated using the following Equation (10):

$$\%ID\ in\ tissue = 100 \times AZM\ content/(administered\ dose \times body\ weight) \quad (10)$$

2.12. Biodistribution of IR783/AZM@FDKP-MPs (pH 4.5)

IR783 is a near-infrared (NIR) dye with good water solubility and is used in NIR imaging to track the distribution of microparticles *in vivo*. Here, IR783 and AZM co-loaded FDKP-MPs (pH4.5) (IR783/AZM@FDKP-MPs, 75 mg kg^{-1}, IR783 10 μg) were prepared and were similarly delivered via intratracheal insufflation, intravenous injection, or intragastric administration in healthy mice to investigate the biodistribution of AZM@FDKP-MPs. The mice were anesthetized and imaged using an *in vivo* imaging system (IVIS®Spectrum, PerkinElmer, US) 5 min, 2 h, 12 h and 24 h post administration. The fluorescence distributions were visualized with the excitation and emission wavelengths at 745 nm and 840 nm, respectively. The major organs (heart, liver, spleen, lung, and kidney) were then excised, washed with saline and visualized using the same set of parameters. Images were analyzed using the Living Image 4.2 (IVIS®Spectrum, PerkinElmer, US).

2.13. Pharmacodynamic study of AZM@FDKP-MPs (pH 4.5) in a mouse model of streptococcus infection

A total of 252 female BALB/c mice were randomized equally into the following six groups (n = 42): (A) control group, (B) immunosuppressive control group, (C) *pneumonia* model group, (D) AZIM@FDKP-MPs powders administrated by intratracheal insufflation, (E) AZM@FDKP-MPs in a PBS solution (pH 7.4) administrated by intravenous injection, and (F) AZM@FDKP-MPs in a PBS solution (pH 7.4) administrated by intragastric administration. All mice were allowed to acclimate for seven days prior to the experiments. To induce immunosuppression in groups B-F, 0.5 mg kg^{-1} of cyclosporine (Novartis) was administered intraperitoneally once a day for three consecutive days. *Pneumonia* models were then established in groups C-F by intratracheal instillation of a 20 μl *S. pneumonia* suspension at a concentration of 6×10^8 CFU mL^{-1}. Dosing started 24 h after the inoculation (Fig. 7) and all groups were dosed at predetermined intervals (6 mice at a time). Specifically, AZM@FDKP-MPs powder (75 mg kg^{-1}) was administrated via intratracheal insufflation every 3 days in group D and AZM@FDKP-MPs PBS solution (pH 7.4) (75 mg kg^{-1}) was administrated every day either via intravenous injection or intragastric route in group E and F, respectively.

Relative body weight, relative lung weight and CFUs of *streptococcal pneumonia* in lung tissues were determined to compare the effects of varying treatments. Mice were sacrificed at 0, 1, 2, 4, 6, 8 and 10 day intervals and lung tissues were immediately harvested and weighed. The left lobes pulmonis were fixed in 10% formalin solution at 4 °C for 24 h and then transferred to ethanol (50%–100%, *v/v*), xylene and paraffin, respectively, for tissue dehydration and paraffin embedding. Five micron sections were prepared with a rotary microtome (YD-202A, Jinhua YIDI Medical Appliance Co., LTD, China), stained with hematoxylin and eosin (H&E), and examined under a light microscope. Images were acquired using a JFMV300CG camera and JFMV controller software (Nan Jing Ji Fei Technology Co., Ltd., Nan Jing, China). The right lung lobes were carefully extracted without removing any bronchi and were homogenized (XHF-D, Scientz, Ning Bo, China) with 1 mL of 0.9% saline. The 50 μL homogenate was transferred into a culture flask and diluted with 5 mL of Todd-Hewitt and Yeast extract (THY) medium. After culturing at 37 °C and 5% CO_2 for 24 h in the incubator, the bacterial density for each lung (per g) was determined by a UV–Vis spectrophotometer (752, JINGHUA Instruments, Shang Hai, China) at 630 nm. Absorbance measurements were compared to the standard curve, which was established by determining the absorbance of the standard Maxwell's tube, to determine the CFUs of bacteria present. Relative lung weight and relative body weight were calculated according to Equations (11) and (12).

$$\text{Relative body weight}(\%) = \frac{W_{body\ t}}{W_{body\ 0}} \times 100\% \quad (11)$$

$$\text{Relative lung weight}(\%) = \frac{W_{lung\ t}}{W_{lung\ 0}} \times 100\% \quad (12)$$

where $W_{body\ t}$ was the weight of each mouse at each time point, $W_{body\ 0}$ was the weight of each mouse at day 3, $W_{lung\ t}$ was the weight of lung tissue at each time point, and $W_{lung\ 0}$ was the weight of lung tissue at day −3.

2.14. Statistical analysis

All experiments were conducted in triplicate and repeated at least three different times. Statistical differences between means were determined by SPSS using the student's t-test where $p < .05$ was considered statistically significant. All values are reported as mean ± SD.

3. Results

3.1. Synthesis and characterization of FDKP

FDKP was synthesized using a three-step reaction (Fig. 1) and confirmed using ^1H NMR (400 MHz, DMSO-d_6, δ), IR (KBr), and EI-MS (Fig. 2). As shown in Fig. 2A, the signals at 8.10 ppm (s, 2H, NH) and 8.45 ppm (s, 2H, NH) indicated the formation of two amide bonds between the FDKP ring structure and the fumaric acid. The synthesis of FDKP was further confirmed by the appearance of amide bond peaks at 3293.3 (s) and 3194.8 (s) in the IR spectrum (Fig. 2B), and the IR peaks (Fig. 2B) between 3200 and 2500 (w) indicated two carboxyl groups on each end of the FDKP molecule. Lastly, the mass spectrum (Fig. 2C) demonstrated three peaks at *m/z*: 451 (100) ($M^+ - H$), 473 (18) ($M^+ - 2H + Na$) and 474 (5) ($M^+ - H + Na$), which corresponded to the molecular peaks of FDKP (M_w 452). Collectively, these tests validated the successful synthesis of FDKP.

3.2. Physicochemical characterization of AZM-MPs, FDKP-MPs and AZM@FDKP-MPs (pH4.5 and 6.4) spray-dry powders

AZM@FDKP-MPs was prepared at different mass ratios (Table 1) of AZM and FDKP and was spray dried at pH 4.5 using the aforementioned parameters. As shown in Table 1, an increase in the proportion of AZM impeded the flowability of the dry powders manifested by an increase in repose angle from 37° to over 48°. Additionally, the theoretical D_{aer90} of the particles also exhibited a

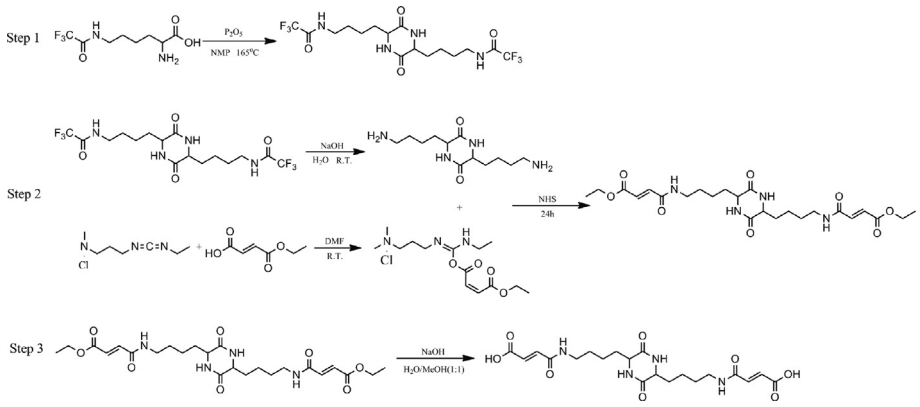

Fig. 1. Synthesis of fumaryl diketopiperazine (FDKP).

slight increase from 4.26 μm at a 1:3 ratio to 4.69 μm at a 3:3 ratio, indicating a reduction of deposition in the lung. On the other hand, an increasing mass ratio contributed significantly to the drug loading of AZM, where an increase from 23.90% to roughly 48.20% was observed. Considering that the antibiotic doses needed are usually high in the treatment of pneumonia, drug loading should be maximized without compromising the flowability too much. The limitation for flowability is the angle of repose <40° or the Carr's index <35% based on U.S. Pharmacopeia, which is considered not as of good flowability but still acceptable for manufacturing [39]. Therefore, a mass ratio of AZM to FDKP of 2:3 was chosen for the rest of the studies.

AZM loaded FDKP dry powders (AZM: FDKP mass ratio at 2:3) were prepared at pH 4.5 and 6.4 and were characterized for particle size, surface morphology, angle of repose, and Carr's index. All the formulations were found to have a high powder yield of over 50% (Table 2). The drug loading of AZM@FDKP-MPs at both pH conditions were close to 40%, as calculated using equation (1). Based on the results from the laser particle size analyzer, the geometric diameter of AZM@FDKP-MPs (pH 4.5 and pH 6.4), as indicated by D_{90}, was smaller than 10 μm with a span value of less than 1.8, indicating a narrow size distribution (Table 2). A large increase in the D_{90} of AZM@FDKP-MPs (pH 4.5 and pH 6.4) was also noted when compared with both FDKP-MPs and AZM-MPs. This may be attributed to the AZM coating on the surface of FDKP-MPs at pH 4.5 or the change in self-assembly at higher pH. Additionally, the surfaces of AZM@FDKP-MPs (pH 4.5 and pH 6.4) were found to be more rough and more porous than AZM-MPs, which decreased particle density. A reduction in particle density has been shown to promote atomization of the particles during inhalation [40]. The D_{aer} of AZM@FDKP-MPs (pH 4.5) also decreased compared to the AZM-MPs and AZM@FDKP-MPs (pH 6.4) as calculated by equation (6). This smaller D_{aer} typically results in increased microparticle deposition into the lung and ultimately improved drug accumulation at the disease site.

To characterize the flowability of the dry powders, the Carr's index and angle of repose were determined and calculated using Equations (4) and (5). As reported in Table 2, AZM-MPs exhibited poor flowability with a Carr's index of almost 50% and an angle of repose over 50° compared with both the blank FDKP-MPs and AZM@FDKP-MPs [39]. Due to their porous structures, FDKP-MPs had a relatively low bulk and tapped density compared to AZM-MPs and AZM@FDKP-MPs. To compare particle morphologies, all formulations were visualized using SEM (Fig. 3). The AZM-MPs (Fig. 3A) appeared spherical and exhibited a much smoother surface than FDKP-MPs and AZM@FDKP-MPs. FDKP-MPs, on the other hand, formed an array of microcrystalline plates in an acidic environment which then self-assembled into microparticles (Fig. 3B) [36,41], with rough surfaces and enhanced surface areas, which is preferable for therapeutic encapsulation. The spherical morphology of AZM@FDKP-MPs showed significant differences when prepared at different pH values (Fig. 3C and D). The surface of AZM@FDKP-MPs (pH 4.5) appeared smoother than FDKP-MPs, which was likely due to the fact that the AZM coating of the MPs filled pores during the spray drying process. In contrast, AZM@FDKP-MPs (pH 6.4) were irregular spherical shapes and displayed significant surface shrinkage.

To determine if microparticles prepared at different pH values resulted in distinct crystalline structures due to different growth mechanisms, the crystallinities of AZM, AZM-MPs, FDKP-MPs and AZM@FDKP-MPs dry powders were analyzed using both X-ray diffraction and DSC. Raw azithromycin showed sharp diffraction peaks across a wide range of values, while only two broad peaks around $2\theta = 10°$ and 18° were observed for spray dried AZM-MPs (Fig. 4A). FDKP-MPs displayed a diffraction peak at $2\theta = 28°$, indicating that FDKP can crystallize in an acidic environment and form microparticles. The same diffraction peak was also observed in the AZM@FDKP-MPs when spray dried at pH 4.5. On the other hand, preparing AZM@FDKP-MPs at pH 6.4 gave rise to a new diffraction peak at $2\theta = 8°$, which indicated that a new crystalline structure was formed. This may be due to a different growth mechanism at this pH.

The DSC thermograms of AZM presented two endothermic peaks at 116.8 °C and 252.6 °C respectively (Fig. 4B), and the same endothermic peaks were observed in the physical mixture of AZM and FDKP. The peak at 116.8 °C disappeared in all spray-dried powders, indicating that AZM became amorphous during the spray drying process. An endothermic peak at 68 °C was observed in AZM-MPs and endothermic peaks at 71 °C and 73.5 °C were observed in AZM@FDKP-MPs prepared at both pH 4.5 and pH 6.4, which corresponded to the melting of amorphous AZM during the spray-drying process. Additionally, FDKP-MPs showed only one endothermic peak at 334.4 °C, which was shifted to 324.3 °C upon spray drying with AZM at pH 4.5. This corresponds to the melting FDKP. The endothermic peak at 334.4 °C disappeared in AZM@FDKP-MPs when spray dried at pH 6.4, which implied that FDKP became amorphous when prepared at pH 6.4.

Hygroscopicity is a measurement of the moisture absorption ability of the microparticles and is known to affect powder cohesion. The hygroscopicity of all formulations was characterized in this study to help optimize particle flowability and deposition. No significant difference in hygroscopicity was observed between AZM and AZM-MPs, with moisture absorption for both formulations below 5% even at 90% relative humidity (RH). Incorporation of FDKP

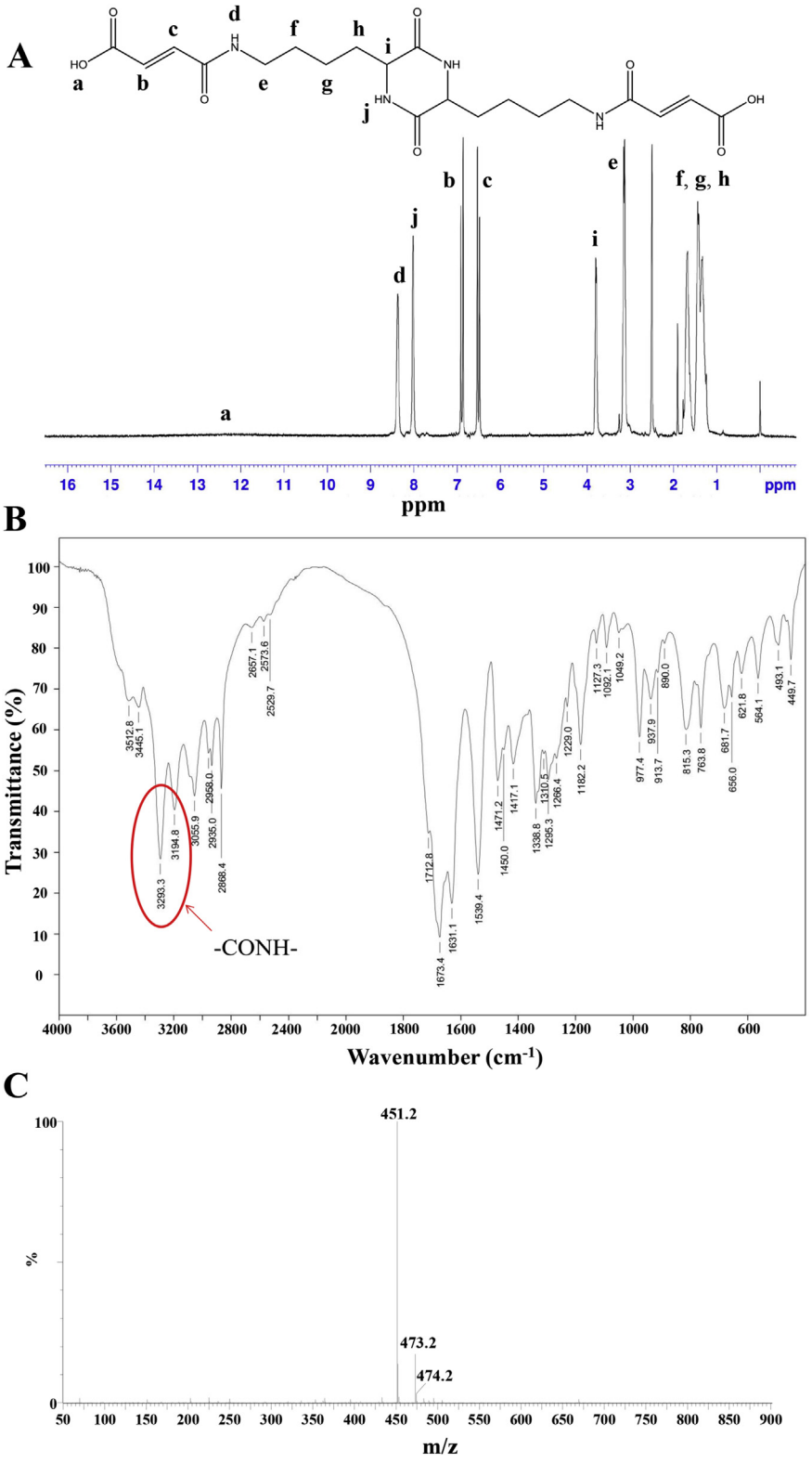

Fig. 2. (A) 1H NMR, (B) IR and (C) MS spectrum of fumaryl diketopiperazine (FDKP).

was seen to increase water absorption across RHs ranging from 50% to 90%, with the largest increase observed by AZM@FDKP-MPs prepared at pH 6.4. Specifically, AZM@FDKP-MPs (pH 4.5) started to show an increase in moisture absorption at a RH as low as 50%. The moisture absorption increased significantly at higher RHs, reaching approximately 15% at 90% RH (Fig. 4C). The hygroscopicity of AZM@FDKP-MPs prepared at pH 6.4 increased almost exponentially as the RH increased. These MPs had a final absorption of more than 40%, which is unfavorable for pulmonary delivery as the particles are more likely to aggregate before reaching the target

Table 1
Laser particle size and flowability parameters of AZM@FDKP-MPs spray-dried at pH 4.5 (mean ± SD, n = 3).

AZI: FDKP Mass ratio	D_{10} (μm)	D_{50} (μm)	D_{90} (μm)	Repose angle (°)	$Daer_{90}$ (μm)	Drug loading (%)
1:3	1.129 ± 0.231	3.271 ± 0.291	8.194 ± 0.319	36.67 ± 0.58	4.26 ± 0.194	23.90 ± 0.10
2:3	1.240 ± 0.076	3.221 ± 0.204	8.255 ± 0.458	39.33 ± 1.53	4.45 ± 0.217	38.63 ± 0.65
3:3	1.297 ± 0.120	3.36 ± 0.186	8.417 ± 0.332	48.67 ± 1.53	4.69 ± 0.173	48.20 ± 0.29

Note: Dx is a parameter to characterize particle size distribution and represents that x % of the particle size lies below Dx.

Table 2
Laser particle size and flowability parameters of AZM, FDKP and AZM@FDKP microparticles (mean ± SD, n = 3).

Formulation	Yield (%)	D_{10} (μm)	D_{90} (μm)	Span value	Repose angle (°)	Carr's index (%)	D_{aer90} (μm)	Drug loading (%)
AZM-MPs	63.37 ± 2.67	1.282 ± 0.125	7.799 ± 0.374	1.657 ± 0.152	52.33 ± 2.89	49.7 ± 0.3	5.24 ± 0.231	/
FDKP-MPs	53.08 ± 2.13	1.042 ± 0.083	5.480 ± 0.212	1.647 ± 0.128	30.67 ± 0.58	29.1 ± 0.2	2.96 ± 0.113	/
AZM@FDKP-MPs (pH4.5)	54.11 ± 1.92	1.240 ± 0.076	8.255 ± 0.458	1.703 ± 0.183	39.33 ± 1.53	37.3 ± 0.2	4.45 ± 0.247	38.63 ± 0.65
AZM@FDKP-MPs (pH6.4)	50.71 ± 4.17	1.962 ± 0.116	10.72 ± 1.56	1.695 ± 0.206	37.33 ± 1.53	32.4 ± 0.4	5.47 ± 0.441	38.93 ± 0.28

site.

3.3. Aerosol performance of spray-dried powders

To investigate the dispersibility and aerodynamic properties of the different formulations, the aerosol performance of the powders was characterized by the Next Generation Impactor (NGI). As shown in Fig. 4D, approximately 20% of any formulation was retained in the capsules or inhalers, which indicated that these particles could be easily aerosolized and passed through the device. In addition, AZM-MPs were found to have a higher deposition at the throat with a much lower fine particle fraction (FPF) of around 38.04% compared with AZM@FDKP-MPs (Fig. 4 D, Table 3). These results suggest a poor inhalation ability of AZM-MPs into the lung. With the incorporation of FDKP, the aerosol deposition in the lung was vastly improved as indicated by greater depositions on stage S_2 to S_4. The FPFs also increased to 64.60% and 53.14% for AZM@FDKP-MPs (pH 4.5) and AZM@FDKP-MPs (pH 6.4), respectively. The mass median aerodynamic diameter (MMAD), an important parameter characterizing the aerodynamic properties of respirable microparticles, was found to decrease from 4.02 μm in AZM-MPs to about 3.8 μm in AZM@FDKP-MPs (pH 4.5 and pH 6.4). More importantly, FPFs for AZM@FDKP-MPs were found to be well over 50%, suggesting that drug accumulation in the deep lung could be highly improved over AZM-MPs alone. Finally, AZM@FDKP-MPs prepared at different pH values showed significant differences in FPF ($p < .01$). According to the NGI evaluation, AZM@FDKP-MPs (pH 4.5) had better aerodynamic properties and achieved more deposition on S_2 to S_4 compared to MPs prepared at pH 6.4, which suggests a more efficient delivery into the deep lung.

3.4. In vitro antibacterial evaluation

In order to evaluate the antibacterial efficacy of microparticles, the minimal inhibitory concentration (MIC) was determined against *S. pneumonia* using a previously reported microdilution method [42,43]. The MIC of each formulation was defined as the lowest concentration that inhibited visible growth of the bacteria after 24 h, and an optical density less than 0.05 was considered as zero bacterial growth in this study. The results *in vitro* demonstrated that FDKP alone did not have any antibacterial effect on S. *pneumonia* (Fig. 5) and that the inhibition of bacterial growth by AZM was dose dependent. The MIC for all AZM formulations tested was determined to be about 0.5 μg mL^{-1}, with no significant differences ($p > .05$) among AZM@FDKP-MPs (pH 4.5), AZM@FDKP-MPs (pH 6.4) and AZM solutions. These results suggest that the incorporation of FDKP did not affect the activity of AZM.

3.5. In vivo biodistribution of azithromycin in mice

The biodistribution of IR783/AZM@FDKP-MPs in mice and the accumulation of particles in the heart, liver, spleen, lung and kidney were visualized using an *in vivo* imaging system 5 min, 2 h, 12 h, and 24 h after particle administration. Fluorescence was observed in the trachea and/or lung at all the time points following intratracheal insufflation (Fig. 6A). In contrast, the fluorescence was found to accumulate primarily in the liver and stomach, respectively, following intravenous injection and intragastric administration, and almost disappeared 12 h post administration (Fig. 6A), indicating the clearance of microparticles occurred faster in both cases compared to intratracheal administration. Examination of the individual organs revealed that the fluorescence intensity in lung tissues remained relatively strong even 24 h after administration (Fig. 6B), an indication of prolonged retention time via pulmonary delivery. In addition, the increase in fluorescence intensity in the liver and kidney with time (Fig. 6A) suggested that the microparticles could eventually be eliminated from the body via biliary and/or urinary excretion when administered intratracheally. On the contrary, a much weaker fluorescence was detected in lung tissues 2 h after intravenous and intragastric administration, indicating much lower particle concentrations and less efficient delivery to the lung. Most microparticles were metabolized or excreted through the liver or kidney as suggested by the relatively strong fluorescence found in both organs in Fig. 6B.

To quantitatively investigate the pharmacokinetics of AZM, AZM content in lung tissues was measured using HPLC at predetermined time intervals following intravenous injection, intratracheal insufflation, or intragastric administration. The results suggested that pulmonary delivery could increase drug accumulation as well as prolong retention time in lung tissues compared with intravenous injection or oral administration. The highest amount of azithromycin in lung tissues was achieved via intratracheal insufflation (4.25 ± 0.73%, 424.69 ± 70.82 μg g^{-1}), which was 3.4 times higher than intravenous injection (1.24 ± 0.33%, 123.73 ± 30.56 μg g^{-1}, $p < .01$) and 10.5 times higher than intragastric administration (0.41 ± 0.13%, 40.57 ± 10.67 μg g^{-1}, $p < .01$) (Fig. 6C). It was also found that a sufficiently high amount of azithromycin (0.17 ± 0.08%, 16.73 ± 7.64 μg g^{-1}, $p < .05$), a concentration significantly higher than the MIC of *S. pneumonia* (0.5 μg mL^{-1}), remained in lung tissues 12 h after intratracheal insufflation compared with the intravenous injection and oral administration, suggesting its potential as a long-lasting treatment for inhibiting bacterial growth. Taken together, it was clearly shown that pulmonary delivery of AZM had significant advantages over both intravenous injection and intragastric administration.

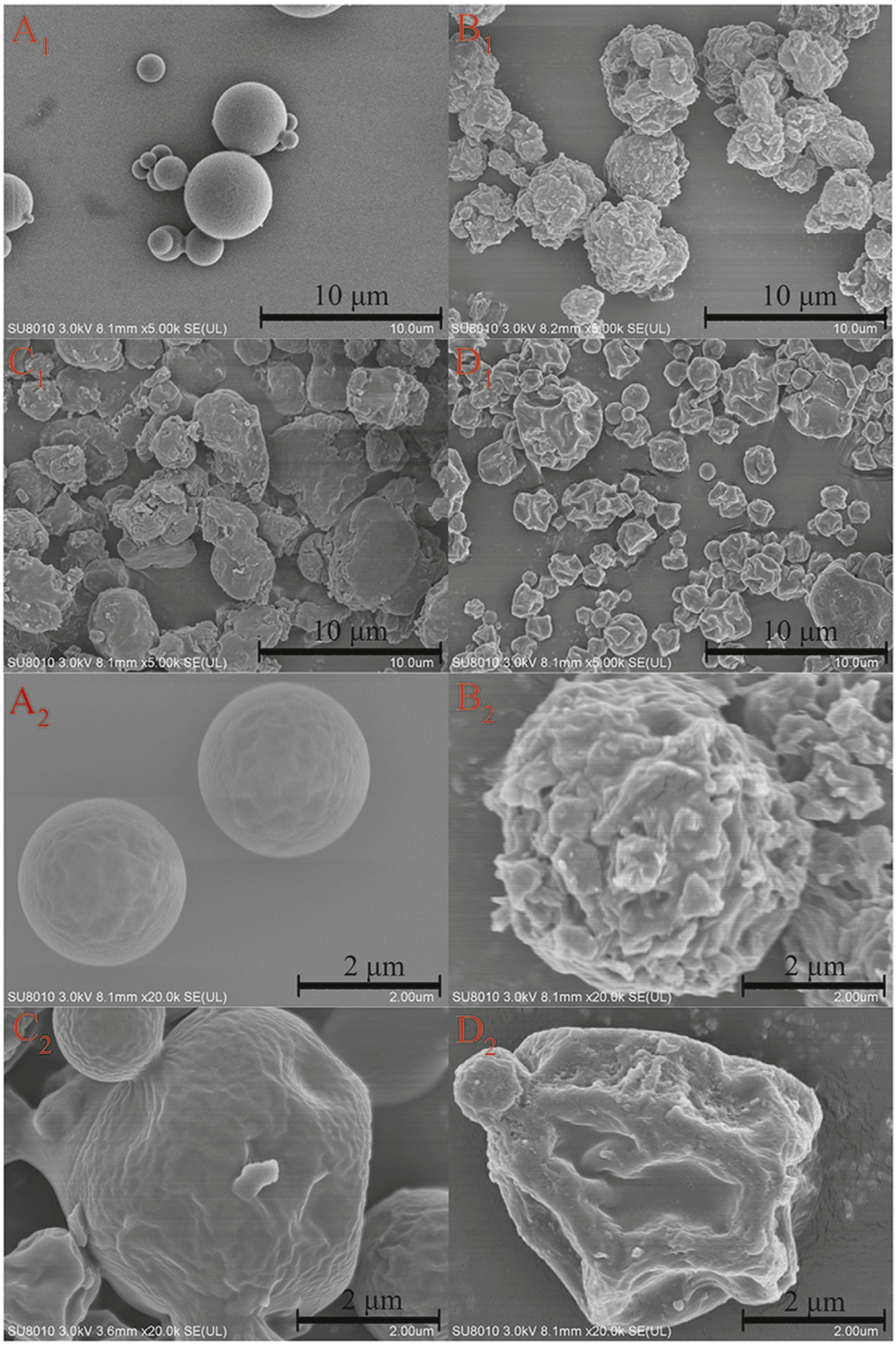

Fig. 3. Scanning electron microscopy micrographs of AZM-MPs (A), FDKP-MPs (B), AZM@FDKP-MPs (pH 4.5) (C) and AZM@FDKP-MPs (pH 6.4) (D).

Specifically, pulmonary delivery maintained higher local concentrations of the antibiotic, potentially reducing both the dosage and frequency of administration for pneumonia treatment.

3.6. Pharmacodynamic study on S. pneumonia

Based on previous studies [44,45], the *streptococcal pneumonia* mouse model can be established by continuous instillation of *S. pneumoniae* solution intratracheally for 24 h. Cyclosporine, an immunosuppressive agent, was used to inhibit immune cell function to allow for *S. pneumoniae* growth and infection [46–48]. Both the relative body weight (Fig. 7A) and the relative lung weight (Fig. 7B) increased steadily in the control group before the *streptococcal pneumonia* infection. Contrarily, a rapid decrease in body weight was observed in groups with the use of an immunosuppressive agent (Fig. 7A). The decrease in body weight was reversed

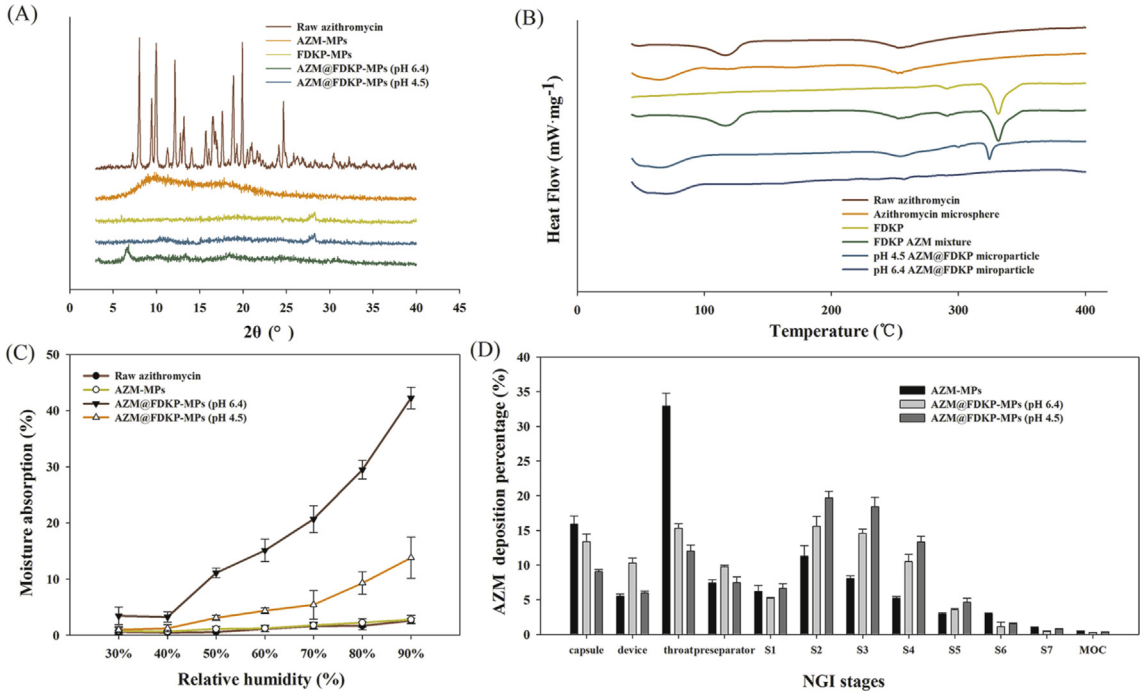

Fig. 4. (A) X-ray diffraction patterns; (B) DSC diagrams; (C) Hygroscopicity and (D) AZM dispersion performance of different formulations. Data = mean +/- SEM; N = 3.

Table 3
Dispersion parameters of AZM@FDKP-MPs.

	AZM-MPs	AZM@FDKP-MPs (pH 4.5)	AZM@FDKP-MPs (pH 6.4)
Emitted fraction/%	84.09 ± 0.28	90.93 ± 0.33$^{**\#\#}$	86.64 ± 0.12**
Fine particle fraction/%	38.04 ± 0.65	64.60 ± 0.41$^{**\#\#}$	53.14 ± 0.38**
Respirable fraction/%	83.79 ± 0.21	89.79 ± 0.09**	89.82 ± 0.06**
MMAD/μm	4.08 ± 0.11	3.82 ± 0.07**	3.84 ± 0.03*
GSD	2.33 ± 0.03	1.88 ± 0.04**	1.87 ± 0.01**

Note: Values represent mean ± SD, n = 3. $^{*}p < .05$ and $^{**}p < .01$ compared to AZM-MPs; $^{\#}p < .05$ and $^{\#\#}p < .01$ when compared to AZM@FDKP-MPs (pH 6.4).

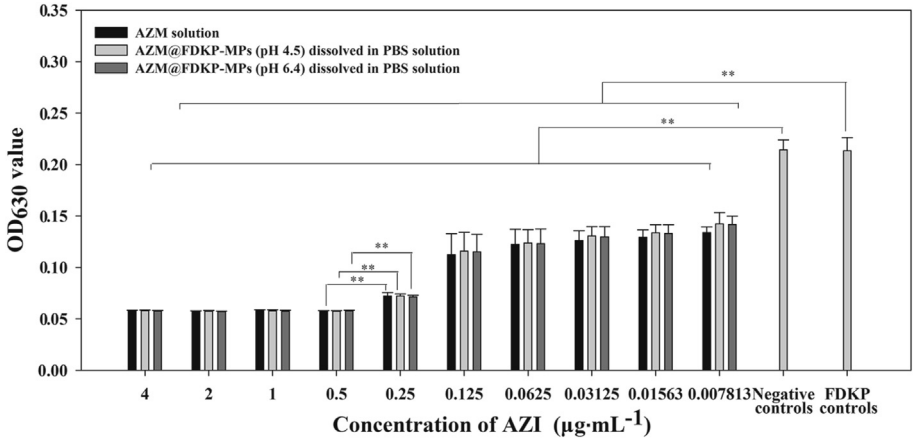

Fig. 5. Growth of *S. pneumonia* when exposed to varying concentrations of AZM and AZM@FDKP MPs. An optical density of 0.05 represents zero bacterial growth. Data = mean +/- SEM; N = 3; ** p <0.01.

in these groups as soon as the dosing of cyclosporine stopped. After one day of AZM administration, the body weight of all treatment groups increased (group D, E and F). The administration of AZM@FDKP-MPs via intratracheal insufflation and intravenous injection both showed significant antibacterial effects as illustrated by the increase in relative body weight as well as the stabilized relative lung weight with respect to time. The relative body weight of mice in the intragastric group did not increase until the second administration, suggesting that a lag time may exist for the oral administration to take effect. To account for the normal growth of

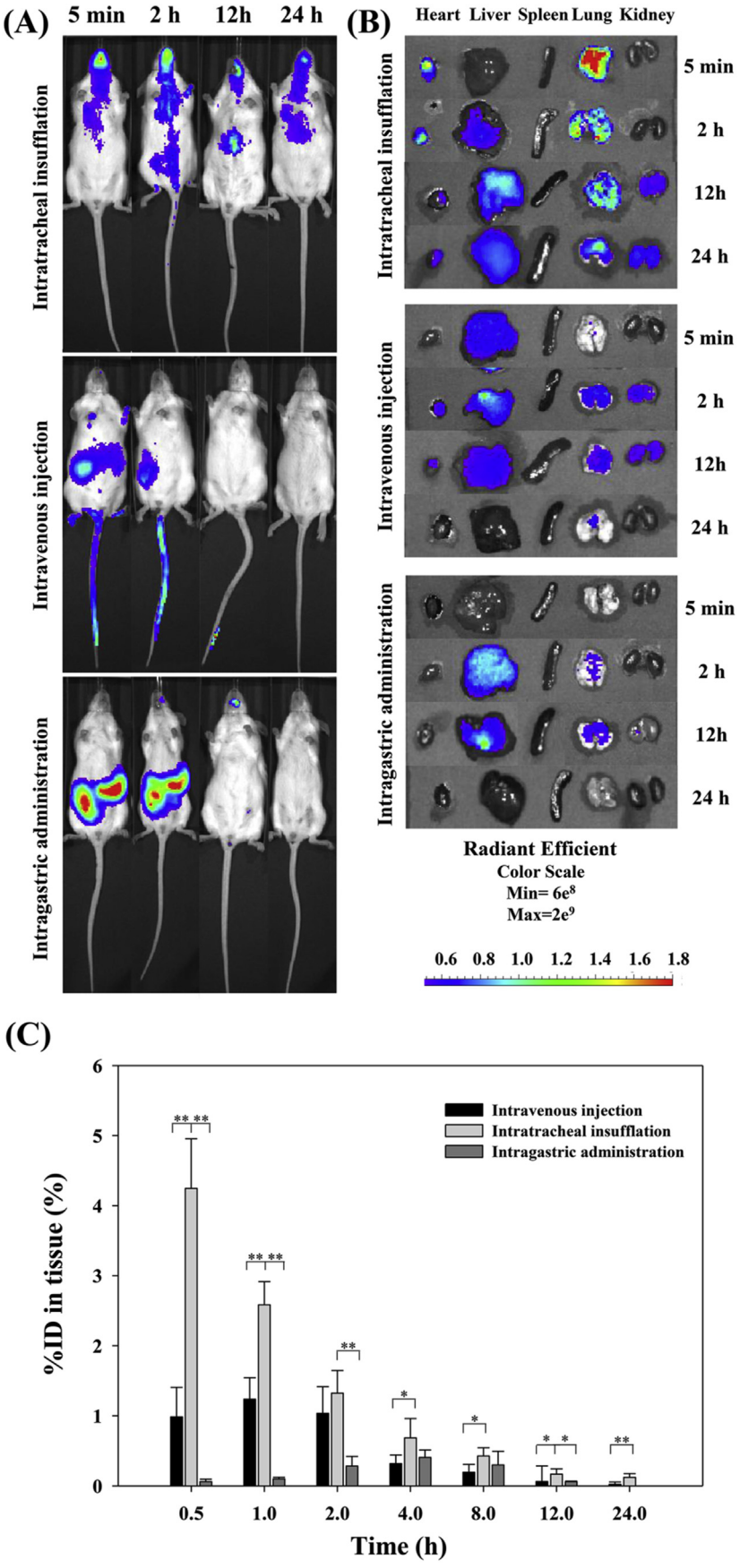

Fig. 6. Biodistribution of IR783/AZM@FDKP-MPs in mice (A) and main organs (B) and AZM deposition in mouse lung tissues (C) at different time points after intratracheal insufflation, intravenous injection and intragastric administration. Values represent mean ± SD, n = 6. *p < .05 and **p < .01.

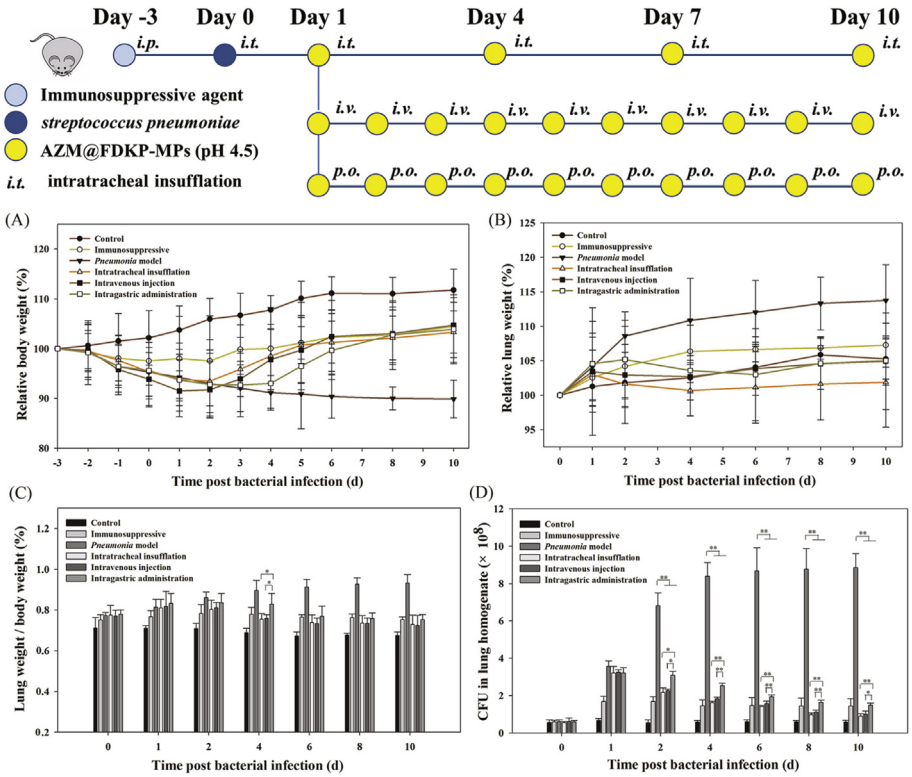

Fig. 7. (A) Relative body weight, (B) relative lung weight, (C) lung weight/body weight and (D) CFU of *streptococcal pneumonia* per gram of lung tissues following different route of administration. Values represent mean ± SD, n = 6. *p < .05 and **p < .01.

mice, the lung weight/body weight ratio was used as an indicator for disease progression. Results showed that only the *pneumonia* model group exhibited sustained increase in the lung weight/body weight ratio (Fig. 7C), while the ratio of all other groups remained stable. A further determination of the CFU of *S. pneumoniae* in lung tissues revealed that there was a significant reduction of bacteria density in both the intratracheal insufflation group and intravenous injection group at day 2 ($p < .05$) and days 4–8 ($p < .01$) compared with the intragastric administration group (Fig. 7D). A time lag of the antibacterial effect was also observed for the intragastric group in which the CFU of *S. pneumoniae* in lung tissues did not decrease significantly until day 4. Finally, it is also worth noting that although there were differences in antibacterial efficacy among treatment groups, all treatments showed significant antibacterial effects compared with the *pneumonia* model group as demonstrated by the significant decrease in CFU of *S. pneumoniae* in lung tissues from day 2–10 ($p < .01$).

To better understand the histopathological changes in lung tissues, lung tissue was H&E stained and analyzed using a light microscope (Fig. 8). The alveoli of the control group (Fig. 8A) and the immunosuppressive group (Fig. 8B) remained intact and were uniform in size. The thicknesses of the alveolar cavity walls also appeared normal and no infiltration of inflammatory cells was observed in alveolar cells, suggesting administration of the immunosuppressive agent alone did not induce *pneumonia*. In contrast, significant inflammatory lesions, thickened alveolar cavity walls and distinct alveolar sizes were all observed in the pneumonia model (Fig. 8C). In mice with pneumonia, the natural structure of alveolar septum disappeared and abundant mucus deposition was discovered to occupy the alveolar space as marked by the black arrows in Fig. 8.

All treatment groups showed distinct inflammation in lung tissues at day one, which further confirmed the successful establishment of the *streptococcal pneumonia* mouse model. One day after administration of AZM, the thickness of the alveolar wall and the alveolar structure recovered rapidly to its original size and shape in the intratracheal insufflation group (Fig. 8D). Inflammatory lesions, such as hyperemia and incrassation, of the alveolar wall were significantly alleviated as well. Most importantly, it was discovered that the incrassation of the alveolar wall almost disappeared and the structure of the alveolar septum was fully recovered five days after administration. Similar therapeutic effects in alleviating the inflammatory lesions were also found in the intravenous injection group (Fig. 8E). In contrast, the alveolar walls remained thickened and the size of alveoli had large variations 1 day after oral administration (Fig. 8F). Significant shrinkage of inflammatory lesions, as well as the recovery of alveolar septum structure, was not observed until 5 days after administration, which was in accordance with previous results that oral administration of AZM had a delayed therapeutic effect.

4. Discussion

As the most commonly used macrolide antibiotic, AZM has been successfully used as a first-line treatment for community-acquired pneumonia for over 15 years [10]. The wide use of antibiotics, however, has raised concerns about the development of antibiotic resistance. Pulmonary delivery has become an attractive method to counteract this trend in that it provides direct access to the lung, supplying increased local therapeutic concentrations with minimal systemic exposure. Unfortunately, AZM-MPs demonstrated poor flowability and aerosolization properties which impeded their application in pulmonary delivery. FDKP, in this study, was chosen as a carrier to vastly improve the aerodynamic properties of the

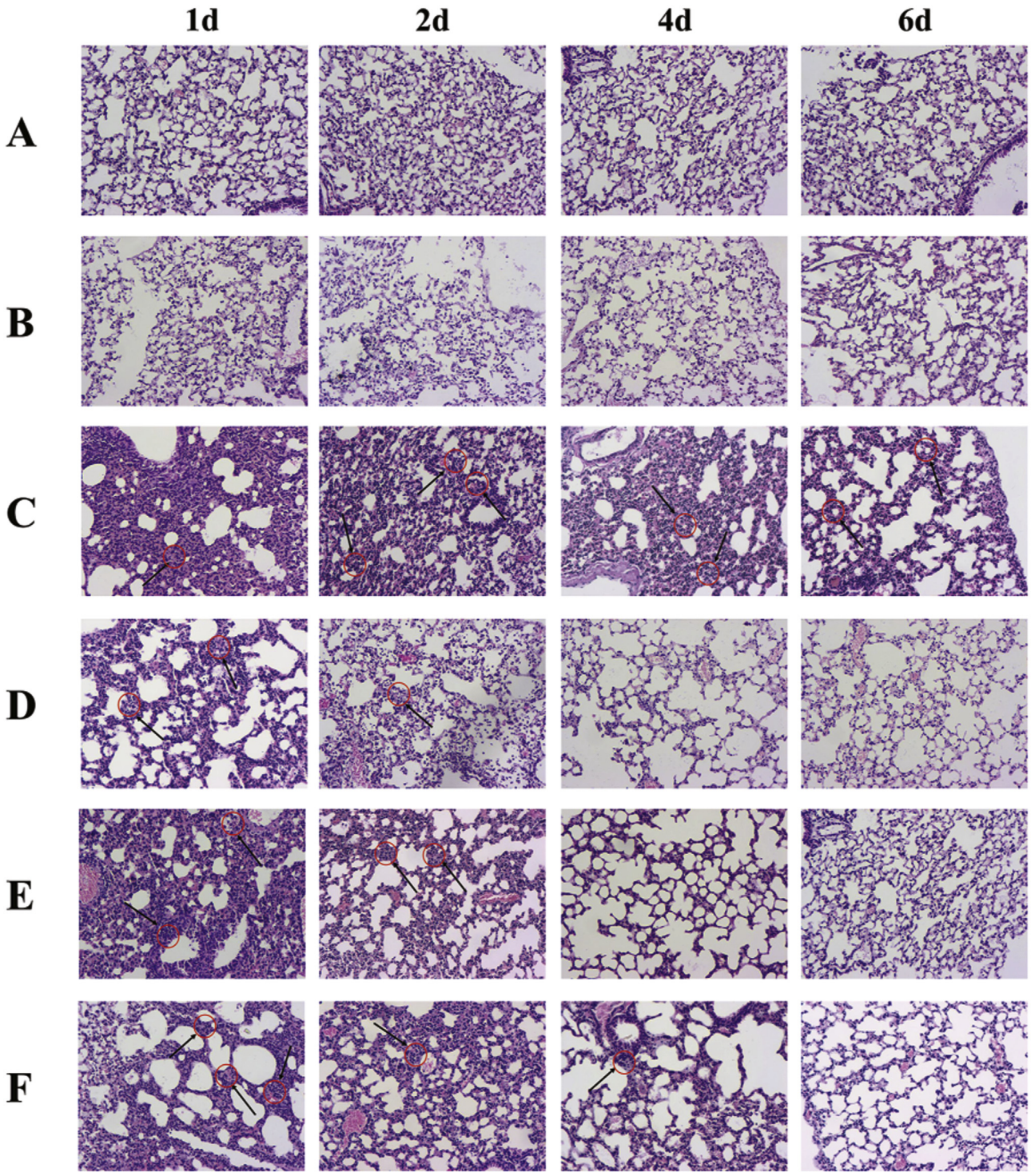

Fig. 8. Histology of lung tissues in control (A), immunosuppressive (B), *pneumonia* model (C), intratracheal insufflation (D), intravenous injection (E) and intragastric administration (F) group 1 d, 2 d, 4 d and 6 d after the establishment of *pneumonia* mouse model. Sections were embedded in paraffin and stained with H & E (magnification 100 ×). Mucus deposition was marked by black arrows.

microparticles and facilitate the pulmonary delivery of AZM. *In vivo* results suggested that the pulmonary delivery of AZM achieved the highest local concentration and prolonged retention time and may represent a successful and novel pneumonia treatment.

FDKP is usually synthesized following a condensation reaction between two trifluoroacetyl (TFA) protected L-lysine. However, the formation of linear by-products significantly decreases the yield of TFA-DKP. The yield can be largely improved to almost 50% with the incorporation of a six-membered ring (N6) in TFA-L-lysine, which provided additional steric hindrance.

To demonstrate the feasibility of using FDKP to improve the pulmonary delivery of AZM, the physicochemical properties and aerosol performance of the spray-dried AZM@FDKP-MPs were investigated extensively. It has been reported that the optimal

aerodynamic diameter for MP deep lung deposition is between 1 and 5 μm [49,50]. Specifically, inhaled particles with a $D_{aer} > 5$ μm will remain in the nose, mouth, or throat, whereas a $D_{aer} < 1$ μm will be exhaled after initial inhalation. More specifically, particles with a D_{aer} between 3 and 5 μm are expected to deposit in the primary or secondary bronchi due to the inertial impaction phenomenon, while particles with a D_{aer} ranging from 1 to 3 μm are capable of reaching tertiary bronchi, bronchioles or even alveoli via sedimentation [24,51]. Using laser particle analysis, the D_{aer90} of AZM@FDKP-MPs was found to be roughly 4 μm and they can therefore be considered good candidates for AZM delivery into the deep lung.

Flowability is also an indispensable part of the particles' aerodynamic behaviors and was therefore characterized by the Carr's index and angle of repose. Results indicated that particle flowability was significantly improved after the incorporation of FDKP. The addition of FDKP to the AZM@FDKP-MP preparation led to particles with lower densities and rougher surfaces compared with AZM-MPs. Of equal importance is the pH; AZM@FDKP-MPs prepared at different pH values showed significant differences in flowability, possibly due to their different geometries or altered surface properties [52]. When prepared at pH 6.4, both FDKP and AZM were dissolved in acetate buffer. FDKP anions attracted AZM cations via electrostatic interactions during spray drying microparticle formation. At pH 4.5, FDKP would first form microparticles in acetate buffer by self-assembly. This was followed by the attraction of cationic AZM, which filled pores on the surface of the microparticles, resulting in much smoother surfaces. In general, rougher surfaces resulted in lower interparticle interactions due to smaller contact surface areas and larger interparticle distances [27]. Finally, the concentration of the surface components of AZM@FDKP-MPs may also affect their flowability. At pH 4.5, the surface of AZM@FDKP-MPs was almost completely covered by AZM as opposed to microparticles at pH 6.4, whose surface contained a mix of FDKP and AZM. This may contribute to decreased intermolecular forces between particles and subsequent prevention of aggregation [53,54]. In summary, it has been clearly demonstrated that the incorporation of FDKP reduced interparticle interactions and thereby improved the flowability of microparticles.

Microparticles were also analyzed for hygroscopicity, an indicator of a material's ability to absorb water as a function of humidity. Water absorption of microparticles can result in local dissolution and recrystallization, which led to irreversible aggregation of the particles though solid bridge formation. This could significantly increase particle sizes and worsen the aerosolization and flowability performance which is vital for optimal aerosol generation and lung deposition [53,55]. The higher hygroscopicity observed in AZM@FDKP-MPs (pH 6.4) compared to AZM@FDKP-MPs (pH 4.5) can be explained by the different particle forming mechanisms at each pH. For example, FDKP was exposed to the surface of the microparticles at pH 6.4, which led to significant water absorption at a high relative humidity. However, at pH 4.5, the FDKP core was protected from its surroundings by the AZM coating, making the microparticle more resistant to water absorption.

To confirm the forming mechanisms when prepared at different pH, the crystallinities of AZM@FDKP-MPs at pH 4.5 and pH 6.4 were determined by X-ray diffraction and DSC, respectively. Raw AZM exhibited a crystalline state, which is exemplified by a series of sharp 2θ peaks in the XRD pattern (Fig. 4A). The diffraction peaks disappeared after spray-drying of AZM, indicating a transition of the crystalline structure to an amorphous state. For FDKP, a sharp peak was observed around 28°, suggesting that FDKP can form a crystalline structure during precipitation at acidic conditions [36]. When precipitating at pH 4.5, it was hypothesized that FDKP microparticles initially formed were followed by the absorption of AZM, which resulted in the same diffraction peak observed in FDKP-MPs as shown in Fig. 4A. For MPs formed at pH 6.4, the shift in 2θ peak suggested a different type of crystalline structure, which further supported the hypothesis that FDKP and AZM could both dissolve at pH 6.4 and form a complex by intermolecular forces during the spray drying process. This change in crystal structure may explain the observed difference in surface morphology of the microparticles and thereby may have contributed to the improvement in flowability and moisture absorption compared to particles formed at pH 4.5.

DSC was also used to further characterize the crystallinities of FDKP-AZM-MPs (pH 4.5 and pH 6.4). Raw AZM always contains bound water. The dehydration of AZM therefore led to the endothermic peak at 116.8 °C. The additional endothermic peak at 252.6 °C can be explained by the degradation of the ring structure. During spray drying, the crystalline structure of AZM changed as illustrated by the shift of endothermic peaks to about 70 °C. When spray-drying with FDKP at both pH 4.5 and pH 6.4, there was no significant shift of the endothermic peaks at around 70 °C and 250 °C, whereas the endothermic peak at 334 °C (represented the melting of FDKP) disappeared when spray dried at pH 6.4. As mentioned before, FDKP and AZM were both soluble at pH 6.4 and can form a complex by intermolecular forces during the spray drying process. This complex may have a higher melting point or transform into an amorphous state, which could explain the disappearance of the endothermic peaks of FDKP.

The aerodynamic properties of MPs were extensively investigated using NGI [56–58]. The aerodynamic properties of MPs are affected by several factors such as particle size, surface properties as well as interparticulate forces (including van der Waals, electrostatic, and capillary forces). AZM-MPs had high surface free energy and could easily adhere to each other via strong interparticulate interactions, which led to particle aggregation and poor re-dispersibility. As a result, most AZM-MPs deposited at the throat. The incorporation of FDKP was hypothesized to improve the dispersion of microparticles by decreasing the intermolecular hydrogen bonding as FDKP has less hydrogen bond donors or acceptors. Indeed, significant improvements in EF, FPF and MMAD were observed in AZM@FDKP-MPs. Furthermore, there were also significant differences in the EF and FPF between particles prepared at pH 4.5 and pH 6.4. We observed a higher deposition on S_2 to S_4 and FPF of AZM@FDKP-MPs (pH 4.5). This may be due to their lower D_{aer90} compared to AZM@FDKP-MPs (pH 6.4), suggesting that AZM@FDKP-MPs (pH 4.5) are potentially easier to inhale into the lung. Based on the above reasons, spray-drying at pH 4.5 was chosen for the AZM@FDKP microparticle preparation.

To evaluate the efficacy of pulmonary delivery of AZM against community-acquired pneumonia, AZM@FDKP-MPs were administered in a mouse model by either intratracheal insufflation, intravenous injection, or intragastric administration. The antibacterial effect of AZM was found to be concentration-dependent and the optimal effect was achieved when drug concentrations were maintained above the MIC. Delivery of AZM by inhalation can therefore theoretically provide better antibacterial effects than intravenous injection or intragastric administration due to higher local drug accumulation as well as longer retention times to maintain MIC. As shown in Fig. 6C, the amount of AZM recovered from lung tissues was 4.25 ± 0.73% (%ID) 0.5 h after intratracheal insufflation, which was more than 4 times higher than intravenous injection (0.98 ± 0.45%, $p < .01$) and more than 70 times higher than intragastric administration (0.059 ± 0.046%, $p < .01$). The AZM concentration in lung tissues was still 0.12 ± 0.05% (%ID) 24 h after intratracheal insufflation as opposed to 0.021 ± 0.013% ($p < .01$) found in intravenous administration and below the detection limit

in intragastric administration. This observation was further supported by *in vivo* imaging of the microparticle biodistribution (Fig. 6B) where much higher fluorescence intensity, an indicator of AZM concentration, was observed in lung tissues 5 min, 2 h, 12 h, and 24 h after intratracheal administration. The higher local concentration and long retention time via intratracheal insufflation were likely due to the fact that it provided direct access to the lung, whereas AZM administered by an intravenous or intragastric route can be rapidly removed by polymorphonuclear leukocytes (PMN) or macrophages after entering the blood circulation [59]. Although the AZM concentrations of AZI@FDKP-MPs (pH 4.5) in lung tissues decreased from 500 μg mL^{-1} to 30 μg mL^{-1} over the course of 24 h, it was still significantly higher than the MICs of bacteria that can cause pneumonia such as *S. pneumonia* (0.5 μg mL^{-1}), *mycoplasma pneumonia* (0.0027 μg mL^{-1}) and *legionella pneumophila* (1.0 μg mL^{-1}) [49].

When bacteria are cultured in the presence of a drug concentration higher than MIC, antibiotic resistance tends to develop with time. To prevent resistance from developing, a novel measurement of resistance, called mutant prevention concentration (MPC), has been proposed [60]. MPC is defined as the threshold above which the selective proliferation of resistant mutants occurs only rarely. The concentration of antibiotics between MIC and MPC is called the bacteria mutant selection window (MSW). When the drug concentration is within the MSW, mutant bacteria will selectively grow and can ultimately lead to the development of antibiotic resistance. While it is hard to maintain an antibiotic concentration higher than MPC for long time periods when administered via oral administration or intravenous injection, it is possible to achieve a higher local concentration than MPC with a smaller dosage of drugs by pulmonary delivery, as demonstrated in the pharmacokinetics study.

To demonstrate that the pulmonary delivery of AZM could improve its antibacterial efficiency *in vivo*, a pneumonia mouse model was established using *S. pneumonia* (ATCC 49619). This model was used to systematically evaluate the pharmacodynamics of various formulations of MPs via different routes of administration. Studies *in vivo* illustrated that the AZM@FDKP-MPs (pH 4.5) administrated by intratracheal insufflation and intravenous injection performed better at inhibiting bacteria growth than intragastric administration. We therefore hypothesized that AZM@FDKP-MPs (pH 4.5) could be inhaled and deposited directly at the lesion site, which helped avoid AZM systemic circulation distribution and also helped maintain higher local drug concentrations (higher than MPC). High concentrations of AZM at the infection site can inhibit the growth of *S. pneumonia* and provide macrophages in the lung more time to eradicate bacteria, thereby alleviating the inflammatory response. Contrarily, oral administration of AZM exhibited a time lag in antibacterial effects as a result of a longer absorption process and lower oral bioavailability. Using oral administration, an AZM concentration higher than the MIC was only maintained for 10 h and the growth of *S. pneumonia* was not entirely stopped, which could easily lead to the development of antibiotic resistance or reoccurrence. Although there was no significant difference in antibacterial efficacy between intratracheal insufflation and intravenous injection, AZM administrated by inhalation reduced the frequency of administration, which could help to improve patient compliance and reduce the possibility that bacteria will develop resistance.

5. Conclusion

Antibiotic dry powder inhalations for targeted pulmonary delivery offer unique advantages in providing direct access to disease sites and minimizing systemic exposure. However, its widespread adoption has been limited by the scarce selection of excipients, as only a few excipients have been approved by the FDA for use as inhalation carriers, such as lactose and 1,2-distearoyl-*sn*-glycero-3-phosphocholine (DSPC). A large number of biocompatible carriers (polymers, metals and cationic materials) commonly used in other routes of administration may not be suitable for pulmonary delivery due to possible long-term toxicity and potential carcinogenicity. In this study, we have demonstrated the use of FDKP, approved by the FDA for insulin delivery, as a safe carrier for the efficient pulmonary delivery of small molecule drugs like AZM. AZM@FDKP-MPs formulated via spray drying exhibited fantastic aerosolization performance, improved moisture resistance and, most importantly, exceptional deep lung deposition. Results i*n vivo* clearly suggested that AZM@FDKP-MPs administered via intratracheal insufflation achieved much higher local concentration and prolonged retention time compared to intravenous injection and oral administration. As such, AZM@FDKP-MPs have the potential to minimize systemic exposure as well as to reduce the dose and/or frequency of antibiotic administration, which may help to minimize the possibility of bacterial resistance. In summary, this research demonstrated an innovative approach of formulating existing therapeutics for targeted pulmonary delivery to better manage bacterial pneumonia. It also shed light on exciting opportunities to utilize existing technologies to overcome the limitations of conventional delivery routes, potentially improving both bioavailability and therapeutic efficacy.

Acknowledgements

This work was supported by the Ministry of Science and Technology of China (NO.2017ZX09101001-005-003), the National Natural Science Foundation of China (NO. 81501579) and (NO. 81673364), the Natural Science Foundation of Jiangsu Province (NO. BK20150702), the Science and Technology Development Fund of Nanjing Medical University (2016NJMU105), the Priority Academic Program Development of Jiangsu Higher Education Institutions and the Postgraduate Research & Practice Innovation Program of Jiangsu Province (KYCX17_0674). The authors would like to thank Ian Harding and Brirendra Chaurasiya for helping to edit the manuscript.

Appendix A. Supplementary data

Supplementary data related to this article can be found at https://doi.org/10.1016/j.biomaterials.2018.01.022.

References

[1] S. Jain, D.J. Williams, S.R. Arnold, K. Ampofo, A.M. Bramley, C. Reed, C. Stockmann, E.J. Anderson, C.G. Grijalva, W.H. Self, Y. Zhu, A. Patel, W. Hymas, J.D. Chappell, R.A. Kaufman, J.H. Kan, D. Dansie, N. Lenny, D.R. Hillyard, L.M. Haynes, M. Levine, S. Lindstrom, J.M. Winchell, J.M. Katz, D. Erdman, E. Schneider, L.A. Hicks, R.G. Wunderink, K.M. Edwards, A.T. Pavia, J.A. McCullers, L. Finelli, Community-acquired pneumonia requiring hospitalization among U.S. Children, N. Engl. J. Med. 372 (2015) 835–845, https://doi.org/10.1056/NEJMoa1405870.

[2] O. Ruuskanen, E. Lahti, L.C. Jennings, D.R. Murdoch, Viral pneumonia, Lancet 377 (2011) 1264–1275, https://doi.org/10.1016/S0140-6736(10)61459-6.

[3] American Lung Association, Trends in pneumonia and influenza morbidity and mortality, Am. Lung Assoc. Epidemiol. Stat. Unit Res. Heal. Educ. Div. (2015) 1–16. http://www.lung.org/assets/documents/research/pi-trend-report.pdf.

[4] C.M. Torio, R.M. Andrews, Statistical brief # 160 national inpatient hospital Costs : the most, Healthc. Cost Util. Proj. 31 (2013) 1–12, https://doi.org/10.1377/hlthaff.2015.1194. Stat. Br. #160 Natl. Inpatient Hosp. Costs Most Expens. Cond. by Payer, 2011.

[5] T. van der Poll, S.M. Opal, Pathogenesis, treatment, and prevention of pneumococcal pneumonia, Lancet 374 (2009) 1543–1556, https://doi.org/10.1016/S0140-6736(09)61114-4.

[6] G.B. Nair, M.S. Niederman, Community-acquired pneumonia: an unfinished

battle, Med. Clin. North Am. 95 (2011) 1143–1161, https://doi.org/10.1016/j.mcna.2011.08.007.
[7] A.D. Petropoulos, E.C. Kouvela, A.L. Starosta, D.N. Wilson, G.P. Dinos, D.L. Kalpaxis, Time-resolved binding of azithromycin to Escherichia coli ribosomes, J. Mol. Biol. 385 (2009) 1179–1192, https://doi.org/10.1016/j.jmb.2008.11.042.
[8] M.N. Lutfiyya, E. Henley, L.F. Chang, S.W. Reyburn, Diagnosis and treatment of community-acquired pneumonia, Am. Fam. Physician 73 (2006) 442–450, https://doi.org/10.1111/j.1651-2227.2012.02648.x.
[9] J.S. Lee, D.L. Giesler, W.F. Gellad, M.J. Fine, Antibiotic therapy for adults hospitalized with community-acquired pneumonia a systematic review, Jama 315 (2016) 593–602, https://doi.org/10.1001/jama.2016.0115.
[10] C.J. Dunn, L.B. Barradell, Azithromycin. A review of its pharmacological properties and use as 3-day therapy in respiratory tract infections, Drugs 51 (1996) 483. https://link.springer.com/article/10.2165%2F00003495-199651030-00013.
[11] W.A. Prescott, G.E. Johnson, Antiinflammatory therapies for cystic fibrosis: past, present, and future, Pharmacotherapy 25 (2005) 555–573, https://doi.org/10.1592/phco.25.4.555.61025.
[12] K. Kasahara, K. Maeda, K. Mikasa, K. Uno, K. Takahashi, M. Konishi, E. Yoshimoto, K. Murakawa, H. Kimura, E. Kita, K. Maeda, Longterm azithromycin therapy for three patients with chronic lower respiratory tract infections, J. Infect. Chemother. 10 (2004) 42–45, https://doi.org/10.1007/s10156-003-0280-4.
[13] L.A. Hicks, T.H. Taylor, R.J. Hunkler, U.S. Outpatient antibiotic prescribing, 2010, N. Engl. J. Med. 368 (2013) 1461–1462, https://doi.org/10.1056/NEJMc1212055.
[14] O. Ciofu, T. Tolker-Nielsen, P. Østrup Jensen, H. Wang, N. Høiby, Antimicrobial resistance, respiratory tract infections and role of biofilms in lung infections in cystic fibrosis patients, Adv. Drug Deliv. Rev. 85 (2015) 7–23, https://doi.org/10.1016/j.addr.2014.11.017.
[15] C.J. Sanchez, P. Shivshankar, K. Stol, S. Trakhtenbroit, P.M. Sullam, K. Sauer, P.W.M. Hermans, C.J. Orihuela, The pneumococcal serine-rich repeat protein is an intraspecies bacterial adhesin that promotes bacterial aggregation in Vivo and in biofilms, PLoS Pathog. 6 (2010) 33–34, https://doi.org/10.1371/journal.ppat.1001044.
[16] J.E. Vidal, H.P. Ludewick, R.M. Kunkel, D. Zähner, K.P. Klugman, The luxs-dependent quorum-sensing system regulates early biofilm formation by streptococcus pneumoniae strain D39, Infect. Immun. 79 (2011) 4050–4060, https://doi.org/10.1128/IAI.05186-11.
[17] L. Hall-Stoodley, J. Costerton, P. Stoodley, Bacterial biofilms: from the natural environment to infectious diseases, Nat. Rev. Microbiol. 2 (2004) 95–108, https://doi.org/10.1038/nrmicro821.
[18] J. Weers, Inhaled antimicrobial therapy - barriers to effective treatment, Adv. Drug Deliv. Rev. 85 (2015) 24–43, https://doi.org/10.1016/j.addr.2014.08.013.
[19] C.W. Park, H.M. Mansour, D. Hayes, Pulmonary inhalation aerosols for targeted antibiotics drug delivery, Eur. Pharm. Rev. (2011).
[20] C. Loira-Pastoriza, J. Todoroff, R. Vanbever, Delivery strategies for sustained drug release in the lungs, Adv. Drug Deliv. Rev. 75 (2014) 81–91, https://doi.org/10.1016/j.addr.2014.05.017.
[21] S. Weber, A. Zimmer, J. Pardeike, Solid lipid nanoparticles (SLN) and nanostructured lipid carriers (NLC) for pulmonary application: a review of the state of the art, Eur. J. Pharm. Biopharm. 86 (2014) 7–22, https://doi.org/10.1016/j.ejpb.2013.08.013.
[22] J.A. Champion, Y.K. Katare, S. Mitragotri, Particle shape: a new design parameter for micro- and nanoscale drug delivery carriers, J. Contr. Release 121 (2007) 3–9, https://doi.org/10.1016/j.jconrel.2007.03.022.
[23] A.T. Florence, J. Siepmann, Modern pharmaceutics volume 1 basic principles and systems, in: New York Inf. Healthc, 2009, pp. 253–310.
[24] M. Klinger-Strobel, C. Lautenschläger, D. Fischer, J.G. Mainz, T. Bruns, L. Tuchscherr, M.W. Pletz, O. Makarewicz, Aspects of pulmonary drug delivery strategies for infections in cystic fibrosis – where do we stand? Expet Opin. Drug Deliv. 5247 (2015) 1–24, https://doi.org/10.1517/17425247.2015.1007949.
[25] P. Muralidharan, M. Malapit, E. Mallory, D. Hayes, H.M. Mansour, Inhalable nanoparticulate powders for respiratory delivery, Nanomed. Nanotechnol. Biol. Med. 11 (2015) 1189–1199, https://doi.org/10.1016/j.nano.2015.01.007.
[26] M.S. Hassan, R. Lau, Feasibility study of pollen-shape drug carriers in dry powder inhalation, J. Pharm. Sci. 99 (2010) 1309–1321, https://doi.org/10.1002/jps.21913.
[27] M.S. Hassan, R. Lau, Inhalation performance of pollen-shape carrier in dry powder formulation: effect of size and surface morphology, Int. J. Pharm. 413 (2011) 93–102, https://doi.org/10.1016/j.ijpharm.2011.04.033.
[28] S. Antoniu, Novel inhaled combined antibiotic formulations in the treatment of Pseudomonas aeruginosa airways infections in cystic fibrosis, Expert Rev. Anti Infect. Ther. 13 (2015) 897–905, https://doi.org/10.1586/14787210.2015.1041925.
[29] P. Du, J. Du, H.D.C. Smyth, Evaluation of granulated lactose as a carrier for DPI formulations 1: effect of granule size, AAPS PharmSciTech 15 (2014) 1417–1428, https://doi.org/10.1208/s12249-014-0166-z.
[30] H. Yu, J. Teo, J.W. Chew, K. Hadinoto, Dry powder inhaler formulation of high-payload antibiotic nanoparticle complex intended for bronchiectasis therapy: spray drying versus spray freeze drying preparation, Int. J. Pharm. 499 (2016) 38–46, https://doi.org/10.1016/j.ijpharm.2015.12.072.
[31] X. Wu, X. Li, H.M. Mansour, Surface analytical techniques in solid-state particle characterization for predicting performance in dry powder inhalers, KONA Powder Part. J. 28 (2010) 3–19.
[32] P.M. Young, A. Sung, D. Traini, P. Kwok, H. Chiou, H.K. Chan, Influence of humidity on the electrostatic charge and aerosol performance of dry powder inhaler carrier based systems, Pharm. Res. 24 (2007) 963–970, https://doi.org/10.1007/s11095-006-9218-8.
[33] A.J. Mickey, I. Gonda, W.J. Irwin, F.J.T. Fildes, Effect of hydrophobic coating on the behavior of a hygroscopic aerosol powder in an environment of controlled temperature and relative humidity, J. Pharm. Sci. 79 (1990) 1009–1014, https://doi.org/10.1002/jps.2600791113.
[34] J.P. Cassidy, N. Amin, M. Marino, M. Gotfried, T. Meyer, K. Sommerer, R.A. Baughman, Insulin lung deposition and clearance following technosphere®insulin inhalation powder administration, Pharm. Res. 28 (2011) 2157–2164, https://doi.org/10.1007/s11095-011-0443-4.
[35] IV N. Kaur, B. Zhou, F. Breitbeil, K. Hardy, K.S. Kraft, I. Trantcheva, O. Phanstiel, A delineation of diketopiperazine self-assembly processes: understanding the molecular events involved in Nε-(fumaroyl)diketopiperazine of L-Lys (FDKP) interactions, Mol. Pharm. 5 (2008) 294–315, https://doi.org/10.1021/mp700096e.
[36] E. Potocka, J.P. Cassidy, P. Haworth, D. Heuman, S. van Marle, R.A. Baughman, Pharmacokinetic characterization of the novel pulmonary delivery excipient fumaryl diketopiperazine, J. Diabetes Sci. Technol. 4 (2010) 1164–1173, https://doi.org/10.1177/193229681000400515.
[37] J. Stevenson, D. Moye-Sherman, Catalysis of Diketopiperazine Synthesis, 2012. https://www.google.com/patents/US8748609. (Accessed 29 December 2017).
[38] X. Li, F.G. Vogt, D. Hayes, H.M. Mansour, Design, characterization, and aerosol dispersion performance modeling of advanced spray-dried microparticulate/nanoparticulate mannitol powders for targeted pulmonary delivery as dry powder inhalers, J. Aerosol Med. Pulm. Drug Deliv. 27 (2014) 81–93, https://doi.org/10.1089/jamp.2013.1078.
[39] U. S. Pharmacopeial Convention, U. S. Pharmacopeia 38/NF 33, U. S. Pharmacopeial Convention, Rockville, USA, 2016, p. 1326.
[40] R. Vehring, Pharmaceutical particle engineering via spray drying, Pharm. Res. 25 (2008) 999–1022, https://doi.org/10.1007/s11095-007-9475-1.
[41] K. Oberg, J. Sulner, M. Grant, Method of Drug Formulation Based on Increasing the Affinity of Crystalline Microparticle Surfaces for Active Agents, 2016. https://www.google.com/patents/US20160151287. (Accessed 29 December 2017).
[42] M. Ballestero-Téllez, F. Docobo-Pérez, J.M. Rodríguez-Martínez, M.C. Conejo, M.S. Ramos-Guelfo, J. Blázquez, J. Rodríguez-Baño, A. Pascual, Role of inoculum and mutant frequency on fosfomycin MIC discrepancies by agar dilution and broth microdilution methods in Enterobacteriaceae, Clin. Microbiol. Infect. 23 (2017) 325–331, https://doi.org/10.1016/j.cmi.2016.12.022.
[43] A. Espinel-Ingroff, A. Fothergill, M. Ghannoum, E. Manavathu, L. Ostrosky-Zeichner, M.A. Pfaller, M.G. Rinaldi, W. Schell, T.J. Walsh, Quality control and reference guidelines for CLSI broth microdilution method (M38-A document) for susceptibility testing of anidulafungin against molds, J. Clin. Microbiol. 45 (2007) 2180–2182, https://doi.org/10.1128/JCM.00399-07.
[44] E. Azoulay-Dupuis, J.P. Bédos, J. Mohler, P. Moine, C. Cherbuliez, G. Peytavin, B. Fantin, T. Köhler, Activity of gemifloxacin against quinolone-resistant Streptococcus pneumoniae strains in vitro and in a mouse pneumonia model, Antimicrob. Agents Chemother. 49 (2005) 1046–1054, https://doi.org/10.1128/AAC.49.3.1046-1054.2005.
[45] J.P. Bédos, V. Rieux, J. Bauchet, M. Muffat-Joly, C. Carbon, E. Azoulay-Dupuis, Efficacy of trovafloxacin against penicillin-susceptible and multiresistant strains of Streptococcus pneumoniae in a mouse pneumonia model, Antimicrob. Agents Chemother. 42 (1998) 862–867.
[46] Dam Viet Cuong, G. Kulcsár, R. Vámos, P. Dán, I. Nász, Interaction of immunosuppressive agents and human adenovirus infection in mice, Acta Microbiol. Hung. 33 (1986) 33–38. http://www.ncbi.nlm.nih.gov/pubmed/3019068. (Accessed 29 December 2017).
[47] H.G. DuBuy, M. Worthington, M.L. Johnson, Effect of an immunosuppressive agent, cyclophosphamide, on chronic lactic dehydrogenase virus viremia of mice, Infect. Immun. 4 (1971) 720–724.
[48] L. Wang, C. Wang, H. Mei, Y. Shen, G. Lv, R. Zeng, P. Zhan, D. Li, W. Liu, Combination of estrogen and immunosuppressive agents to establish a mouse model of candidiasis with concurrent oral and vaginal mucosal infection, Mycopathologia 181 (2016) 29–39, https://doi.org/10.1007/s11046-015-9947-5.
[49] H.M. Courrier, N. Butz, T.F. Vandamme, Pulmonary drug delivery systems: recent developments and prospects, Crit. Rev. Ther. Drug Carrier Syst. 19 (2002) 425–498, https://doi.org/10.1615/CritRevTherDrugCarrierSyst.v19.i45.40.
[50] M.D. Louey, M. Van Oort, A.J. Hickey, Aerosol dispersion of respirable particles in narrow size distributions produced by jet-milling and spray-drying techniques, Pharm. Res. 21 (2004) 1200–1206, https://doi.org/10.1023/B:PHAM.0000033007.27278.60.
[51] K. Kho, K. Hadinoto, Dry powder inhaler delivery of amorphous drug nanoparticles: effects of the lactose carrier particle shape and size, Powder Technol. 233 (2013) 303–311, https://doi.org/10.1016/j.powtec.2012.09.023.
[52] M.P. Flament, P. Leterme, A. Gayot, The influence of carrier roughness on adhesion, content uniformity and the in vitro deposition of terbutaline sulphate from dry powder inhalers, Int. J. Pharm. 275 (2004) 201–209, https://doi.org/10.1016/j.ijpharm.2004.02.002.
[53] V. Vartiainen, L.M. Bimbo, J. Hirvonen, E.I. Kauppinen, J. Raula, Drug

permeation and cellular interaction of amino acid-coated drug combination powders for pulmonary delivery, Int. J. Pharm. 504 (2016) 89–97, https://doi.org/10.1016/j.ijpharm.2016.03.052.
[54] K. Kawakami, C. Sumitani, Y. Yoshihashi, E. Yonemochi, K. Terada, Investigation of the dynamic process during spray-drying to improve aerodynamic performance of inhalation particles, Int. J. Pharm. 390 (2010) 250–259, https://doi.org/10.1016/j.ijpharm.2010.02.018.
[55] J. Raula, F. Thielmann, J. Kansikas, S. Hietala, M. Annala, J. Seppälä, A. Lähde, E.I. Kauppinen, Investigations on the humidity-induced transformations of salbutamol sulphate particles coated with L-leucine, Pharm. Res. 25 (2008) 2250–2261, https://doi.org/10.1007/s11095-008-9613-4.
[56] B.P. Sullivan, N. El-Gendy, C. Kuehl, C. Berkland, Pulmonary delivery of vancomycin dry powder aerosol to intubated rabbits, Mol. Pharm. 12 (2015) 2665–2674, https://doi.org/10.1021/acs.molpharmaceut.5b00062.
[57] B. Cuvelier, P. Eloy, C. Loira-Pastoriza, B. Ucakar, A.A. Sanogo, C. Dupont-Gillain, R. Vanbever, Minimal amounts of dipalmitoylphosphatidylcholine improve aerosol performance of spray-dried temocillin powders for inhalation, Int. J. Pharm. 495 (2015) 981–990, https://doi.org/10.1016/j.ijpharm.2015.10.019.
[58] Q. Zhou, S.P. Sun, J.G.Y. Chan, P. Wang, N. Barraud, S.A. Rice, J. Wang, J. Li, H.K. Chan, Novel inhaled combination powder containing amorphous colistin and crystalline rifapentine with enhanced antimicrobial activities against planktonic cells and biofilm of Pseudomonas aeruginosa for respiratory infections, Mol. Pharm. 12 (2015) 2594–2603, https://doi.org/10.1021/mp500586p.
[59] C.H. Ballow, G.W. Amsden, Azithromycin: the first azalide antibiotic, Ann. Pharmacother. 26 (1992) 1253–1261, https://doi.org/10.1177/106002809202601014.
[60] G. Sindelar, X. Zhao, A. Liew, Y. Dong, T. Lu, J. Zhou, J. Domagala, K. Drlica, Mutant prevention concentration as a measure of fluoroquinolone potency against mycobacteria, Antimicrob. Agents Chemother. 44 (2000) 3337–3343, https://doi.org/10.1128/AAC.44.12.3337-3343.2000.